THE UNIVERSITY OF HULL

Investigations into the electrical properties of hybrid memristor devices containing surface modified zinc oxide nanorods.

being a thesis submitted for the degree of
MSc Physics (by Research)
In the University of Hull

by

Benjamin Gardner
January 2016

Contents

Abstract

This thesis focusses on improving the fabrication and electronic switching properties of hybrid memristor devices that have been developed in the nanophysics group at the University of Hull. The devices consist of vertically aligned semiconducting ZnO nanorods embedded within an organic polymer (Polymethyl-methacrylate) matrix. They are made using a novel ultra-fast microwave fabrication technique, which provides a simple and cost effective route to the fabrication of devices in large numbers and on lightweight and flexible substrates.

The primary aim of this work was to improve the resistance on/off ratio in the memristors by modifying the ZnO surface stoichiometry. The nanorods high surface area to volume ratio is expected to be important in the switching since it has been shown that the mobility of defects at surfaces of transition metal oxides is much higher than in the bulk. Thus it is possible that either oxygen vacancies and/or zinc interstitials confined on the surface of the ZnO shuttle up and down along the lengths of the nanorods to mediate the switching. Investigations are focussed on the modification of the nanorod surface through oxygen plasma treatment as well as studying changes in the electrical performance of the nanorods by changing the nanorod diameter.

Investigations into the effects of exposing the nanorods to an oxygen plasma showed increased resistance of both the high and low resistive states (HRS/LRS) of devices. Energy Dispersive X-Ray spectroscopy results indicated that a likely cause of the increased resistance is increased oxygen in the nanorod surface, producing a more stoichiometric (ZnO_2) and resistive material.

Attempts at manipulating the overall surface stoichiometry through changes in the surface area to volume ratio, implemented by changing the nanorods diameter, was not successful with the approach used in this work. This was because the nanorod diameter could not be significantly modified through the technique of changing the annealing temperature of the nanocrystal seed layer. This was unexpected as it has been previously reported that the nanorod diameter can be varied between 40nm and 350nm by annealing the seed layer at temperatures between 150°C and 500°C respectively[32].

It is worth noting throughout the investigations that the use of low incidence X-ray diffraction measurements on the thin-films proved to be a quick and reliable way to confirm nanorod alignment and growth along the C axis.

Acknowledgements

Dr Neil Kemp. - Project supervisor, who started the project and constantly directed me on the right path.
Dr Emanuele Verrelli. - Post Doc', helped me ask myself the right questions in an investigation.
Dr Timothy Prior. - Allowed me to use his XRD, and gave me invaluable insight in the results I gathered.

Technical Staff.
Mr Graham Randerson. - Allowed me to use the teaching lab equipment, whenever I wanted!
Mr Garry Robinson. - Brilliant SEM work, EDX work, and tea brewing. Had some of the best days stuck in a dark room looking at grainy images of nanorod samples.

Fellow Students.
Mr Robert Gray. - Leading Ph.D student in this project, got me on track in the beginning, and showed me everything he knew.
Mr Simon Fellows. - Ph.D student. Retaught me the basics of XRD analysis.
Mr Joseph Heward. - Mphys student in this project. Showed me exactly how I shouldn't handle a stressful situation.
Mr Josh Stimson. - Mphys student. Kept me sane with nights out, distractions, and general shenanigans!

The Physics and Mathematics department admin team and their endless supply of sweets!

List of Figures

List of Tables

Chapter 1, Introduction

Memristors (or resistive memories) are a new form of non-volatile memory that operate via switching between two different resistive states when a voltage pulse is applied. They have particular advantage in computing because they combine the high speed and high density of Static Random-Access Memory (SRAM) and Dynamic Random-Access Memory (DRAM) with the non-volatile operation of FLASH memory and so have the potential to replace conventional types of solid state memory. The theoretical foundation of the memristor was conceived in the early 1970's by Leon O. Chua of the University of California[1]. Chua's paper, "Memristor - the missing circuit element" was published in 1971 and ultimately described a circuit component that did not exist. However, since the 1960's certain materials have been known to exhibit resistive switching behaviour but there was no link between their switching mechanisms and Chua's theory. In 2008 a breakthrough was made by R. Stanley Williams and colleagues at Hewlett-Packard Laboratories when they linked switching in TiO_2 with the memristor theory developed by Leon Chua nearly 4 decades prior. This re-invigorated the field of resistive switching devices and transformed the field into an important emerging technology as highlighted in a recent report from the International Technology Roadmap for Semiconductors[2]

Historical Perspectives

The memristor as a two terminal circuit component has been described by Leon O. Chua as the fourth basic circuit component after resistors, capacitors and inductors[3]. It exhibits notable different behaviour to that of the other three components, such as the fact that its present resistance is dependent on previous charge flow through the device even when it is not powered. So it can be said that the device remembers its history, remembering its most recent resistance until it is powered again[4]. In 2008, patents were issued for memristors to be included in neuromorphic computing and other neural frameworks by the Hewlett Packard Development Company using molecular junction nanowires[5], which is a memristor based multi-level memory device which also utilises resistor arrays[6]. These neuromorphic computing architectures have a strong relevance in industry to be used as a core framework for multisensory integration in automated systems where it would be important to detect movement, recognise items visually, or use other sensors to

detect sound, chemicals, radiation, and other external stimuli. This neuromorphic computing is a concept that ties analogue circuitry with the electrical characteristics of neurons and synapses responsible for a range of activities in the brain, such as memory, muscle control, and sensory perception.

These novel devices are beginning to meet the necessary requirements of performance needed for commercialization as ascribed by the key performance indicators (KPI) of endurance memory retention and speed. In 2011 devices based on titanium dioxide[7] first achieved repetitive switching endurances of 10^4 - 10^6 times greater than those performances seen in flash memories. A more recent advancement that is in the final stages of development is a device known as The Machine[8]. This computer, being developed at the Hewlett Packard Development Company, meets all three KPIs and has been heralded as an entirely new type of computer, one in which memory and storage are fused together. If successful this new architecture could potentially revolutionize computing. The Machine utilises cores comprising of memristor banks and advanced photonic links[9] and is expected to be built using a truly three-dimensional computing architecture, as opposed to the more commonplace Copper/Silicon two-dimensional architecture seen in everyday computers. Also recently in memristor research there has been a strong movement towards neuromorphics, which aims to build brain like systems with devices that can hold more than the conventional 2 (binary) states. Currently devices have been shown to be able to hold up to 6 states[10] with a clear framework for expansion to many more, such as 10 to form a base 10 framework. Memristor neuromorphics main advantage over traditional systems however, is its ability to avoid computational bottlenecks[11] present in current von Neumann architecture machines (typical examples being modern common computers). The focus of neuromorphics (non von Neumann architecture) is to emulate a system similar to a mammalian brain, the parallel processing ability coupled with the ability for rapid energy dissipation. From this the goal would be to create networks and circuits that learn, and vastly improve current computers capacities of pattern recognition vital to process details in speech and images.

Moore’s law, although not strictly a physical law, is a relationship that was observed and described by Gordon E. Moore, cofounder of Intel and Fairchild Semiconductor, in 1965 and subsequently named after him. The relationship

describes[12] the fact that the number of transistors on an integrated circuit double approximately every two years. This description has taken other forms stating computing power doubles every two years, or the physical sizes of devices shrink ever couple of years, ultimately they all describe the same thing. This has largely remained true 50 years and recently has expected to come to an end due to current limitations in fabrication and the physical limits of nanoscale devices such as current retention and nanoscale circuit resolutions. Intel has reported a slowing in the pace of advances recently[13], stating that current decelerations are "a natural part of the history of Moore's law.[14]" Memristor technology will likely extend the life of this two year trend in technology, allowing more powerful machines to be built.

Memristors

The field of memristors was born from Leon Chua's appreciation of the symmetrical relationships between the four fundamental circuit variables: current (i), voltage (v), and their respective time integrals charge (q) and flux linkage (ϕ). Leon Chua[15] showed that *"any 2-terminal black box with two electrical terminals is a memristor if it obeys the following state-dependent Ohm's law.*

Current-controlled state-dependent Ohm's Law:

$$v = R(x)i$$

$$\frac{dx}{dt} = f(x, i)$$

If the current i is the input, or

Voltage-controlled state-dependent Ohm's Law:

$$i = G(x)v$$

$$\frac{dx}{dt} = g(x, v)$$

If the voltage v is the input"

Excerpt 1 – Memristors are defined by a state dependent Ohm's law, Chua, L. O. 2013, "Memristor, Hodgkin–Huxley, and Edge of Chaos", Nanotechnology 24, 383001.

In the above, R(x) and G(x) are both scalar variables, and are attributed to the memristance (memory resistance) and the memductance (memory conductance) respectively. These are given the usual units for resistance and inductance, Ohms and Siemens. In the above, x represents an internal physical parameter (such as temperature), f(x,i) and g(xv) are Lipchitz functions dependent on the internal physical parameter and current/voltage.

The memristance is dependant of the time integral of the current, as such the present state of the device is dependent on its history. The same can be said of its memductance, with the exception that here it is a time integral of the voltage.

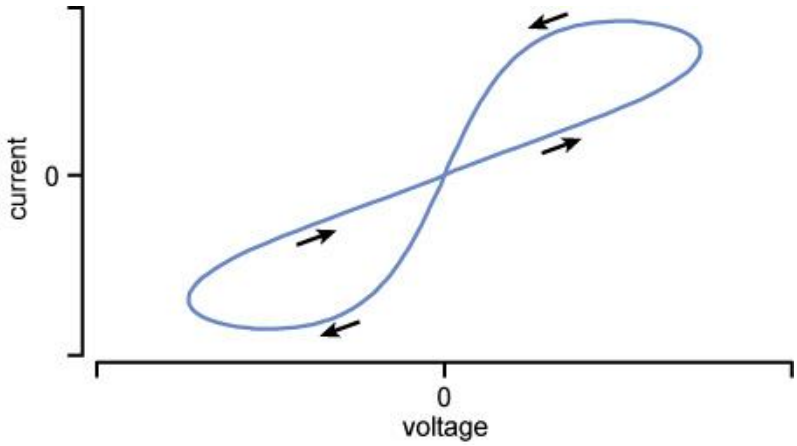

Figure 1 - An example of a pinched hysteresis loop on a current/voltage graph.

Figure 1 shows a double-valued hysteresis loop passing through the origin, also known as a pinched hysteresis loop it shows the typical current/voltage behaviour of a memristor. The idea behind it is that each loop deforms as the frequency, or the amplitude, of the input waveform changes[9]. This behaviour subsequently can vary with the input waveform, amplitude and frequency, so can produce a range of hysteresis loops with varying shape. If there was a positive or negative voltage offset, the loop pinch drift would from the origin, so the above figure cannot be considered to be an overall representation of all memristor behaviour.

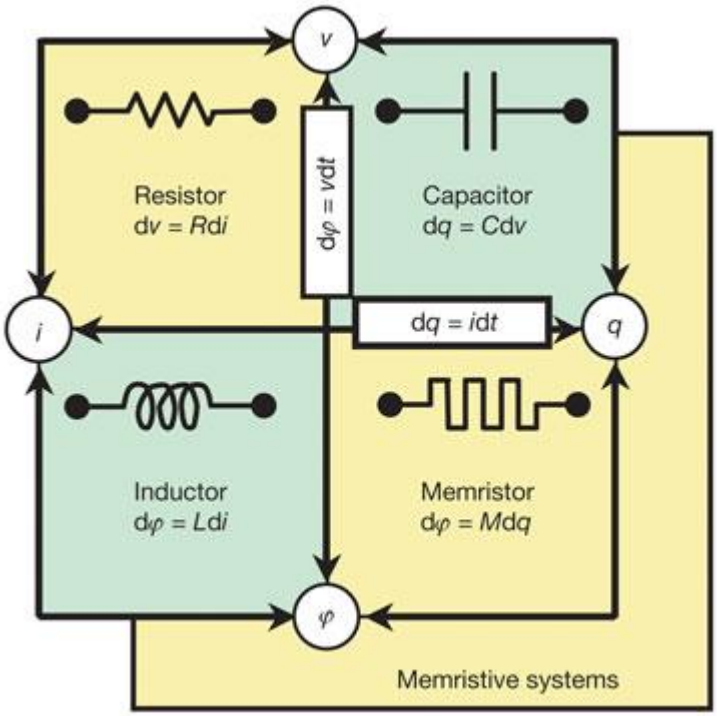

Figure 2 - Memristors, the fourth circuit element, linking charge and flux.

After resistors, capacitors, and inductors, memristors have become the fourth basic circuit component forming a relationship between electric charge and magnetic flux. They are broadly defined as two terminal non-volatile memory devices based on resistive switching, this would include devices such as Magneto-Resistive Random Access Memory (MRAM) and Resistive Random Access Memory (RRAM)[16]. This relationship of similar behaviour between memristors, as an individual circuit component, and Random Access Memory as a fully developed device comprised of many full circuit architectures leads naturally to the concept of a memristor based random access memory device. Such a device which is similarly characterised as the known devices above as non-volatile) has been shown to have a superior read time, with a more efficient power consumption[17]. There are two main types of memristors, electrochemical metallisation memory (ECM) cells, and valence change mechanism memory (VCM) cells. In ECM cells it is the metal electrodes which become oxidised, these ions then migrate to the opposing electrodes forming pure metal filaments connecting the electrodes. In VCM cells both metal and oxygen ions travel, forming a semiconducting filament between the electrodes. Oxygen ions in VCM consist of both negatively charged ions and positively charged oxygen vacancies[18].

Resistive Switching in Metal Oxides

Metal oxides with their semiconducting properties are vital in all modern day circuity most notably as the basis of nano-scale transistor processor chips, the core of all computing devices. Hysteretic I/V behaviour in a metal-insulator-metal (MIM) device of Al / Al_2O_3 / Al was first reported by Hickmott[19] in 1962 using aluminium oxide. This report indicated that resistive switching occurred as a result of an applied electric field.

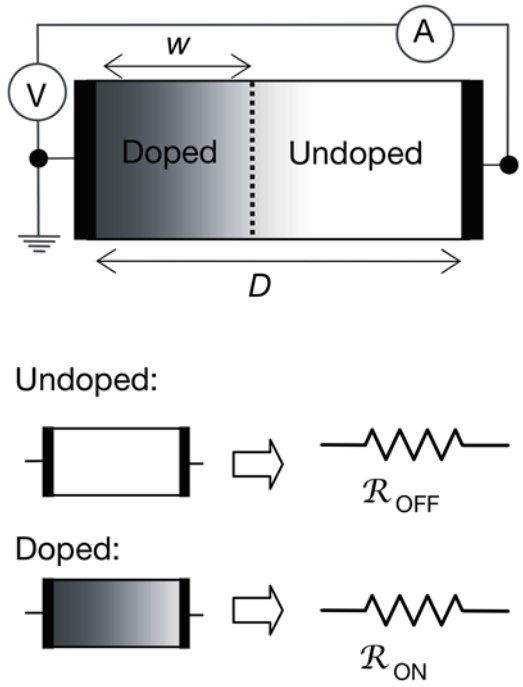

Figure 3 - HP memristor, illustrating how the ratio of the two regions can be altered[20]

TiO_2 is also a notable candidate for memristive devices, since switches based on this dielectric show the pinched hysteresis loop i-v behaviour. A metal-oxide-metal device comprised of platinum and titanium dioxide was shown to require exponentially less energy to switch as current was increased[21], these devices were formed on silicon substrates. The main physical switching mechanism for these bipolar oxide switches is a stoichiometric difference in the TiO_2 layers[22]. The physical structure as described by HP Labs in Figure 4 shows the bottom electrode contains oxygen vacancies, allowing this layer to conduct more than the upper layer which is an electrical insulator. It is the interfaces between these materials that allow vacancies to drift in a particular direction under an external electric field. There is Ohmic conduction at the interface between the bottom layer of TiO_2 and Pt because of the oxygen vacancies. At the top layer there is

a Schottky barrier between the metal - semiconductor junction and this serves as a diode. The drift in vacancies from a positive electric field changes the interfaces between these TiO_2/Pt junctions, mainly the top layer where the Schottky barrier collapses due to the presence of the excess vacancies allowing Ohmic conduction and switching the device into an ON state. When a negative field is applied, the opposite is true and the vacancies reverse, reforming the Schottky barrier and switching the device into the OFF state[23].

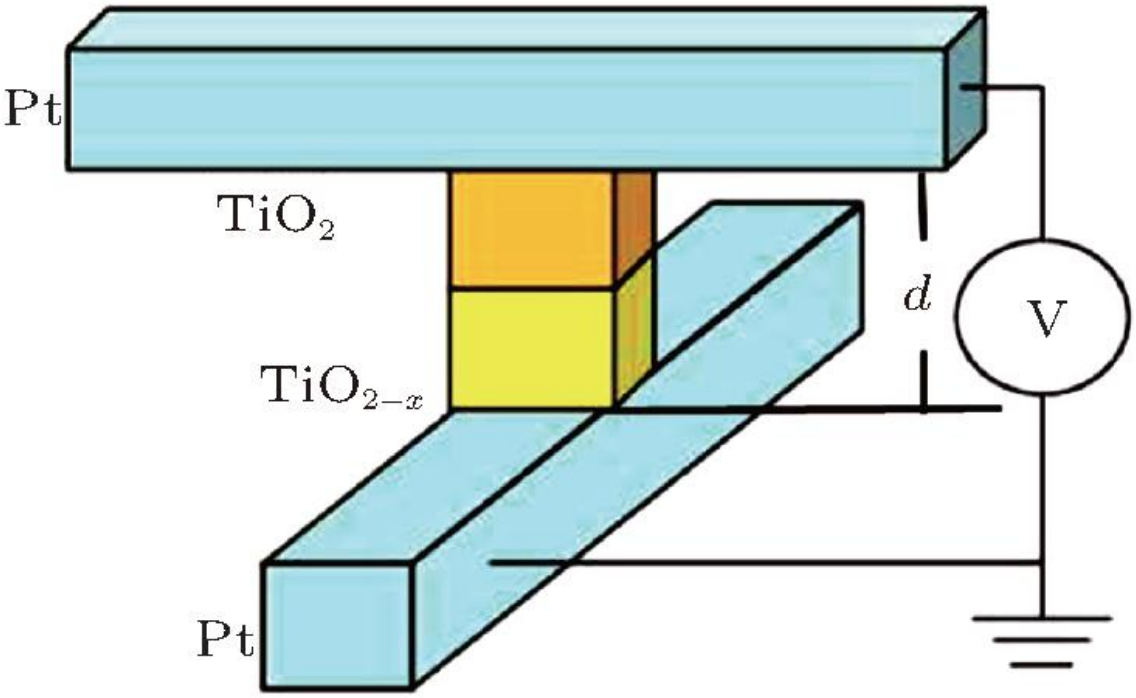

Figure 4 – The structure of a Pt/TiO2/Pt memristor [24]

Controversies mainly tied to these attempts to understand memristive oxide switches are largely due to a lack of a predictive compact model that can be integrated into common simulation packages. Such models have not become available despite massive advancements in the collective understanding of physical switching mechanisms in Ohmic and ionic conductors [21, 25].

Zinc oxide

ZnO, with a bandgap of 3.3eV and its wurzite structure (Figure 5), is an ideal n-type semiconductor. The background free electrons arise from a deviation in the general stoichiometry of the crystals leading to the presence of intrinsic defects such as oxygen vacancies. ZnO as a semiconductor was last heavily researched in the 1970's through to the early 1980's and has now seen a

resurgence with an increased interest in displays, optoelectronics, radiation resistant electronics, and spintronics[26].

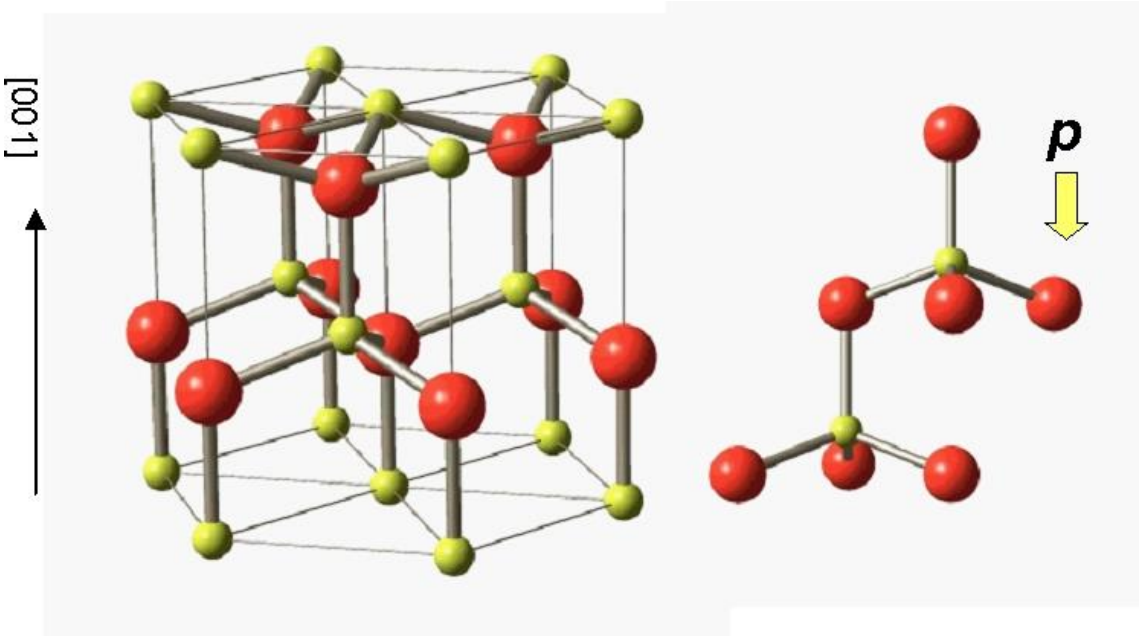

Figure 5 – ZnO wurzite cell structure.[27]

The primary conduction mechanisms observed in ZnO based devices are similar to the mechanism described above for the titanium dioxide based devices. These mechanisms of electronic conduction responsible for the switching are still under considerable debate, however it is well known that resistance can be changed with alterations to the applied electric field. Two mechanisms occur with these types of devices; hopping conduction occurs in the high resistive state (HRS) and is associated with carrier tunnelling in the oxide bulk. Ohmic conduction (or filamentary conduction), in the low resistive state (LRS)[28], is attributed to the formation of conductive filaments connecting the two electrode/ZnO interfaces across the device, both of these mechanisms are bulk-limited. Because of this, it was a clear aim to target a device that utilised efficient nanostructures, such as nanorod forest formations. It is speculated that nanorod architectures could be used to form localized regions of high electric field which could be used to control the switching at the metal electrode/ZnO nanorod interface regions. This could potentially lower the voltage and increase the speed of switching in the devices.

Organic and Hybrid Memristor Device

Organic memristor devices (OMD's) are typically based on either small organic materials such as tetracene[29], or thin polymer films of active organic materials sandwiched between two metal electrodes similar to metal oxide devices.
The main mechanism for switching in these systems is filamentary (Ohmic) conduction such as that seen in metal oxide switches. A typical example of an organic device that switches via the filamentary conduction mechanism is a metal/poly(methyl-methacrylate-co-9-anthracenyl-methacrylate)/metal based device. The polymer was shown to retain binary information and behaves predominantly like a thyristor acting as a bistable switch depending on the direction of current flow, it was also shown that it has a switching performance of 0.5ms with an endurance of switching thousands of times[30].
An example of a device that most likely does not switch via the filamentary conduction mechanism is metal/2-Amino-4,5-imidazoledicarbonitrile/metal[30].
The mechanism behind these organic bistable devices (OBD's) is still under investigation since they still show some Ohmic behaviour. However this polymer was predominantly used to make OBD's, unlike our devices, these OBD's were fabricated through thermal evaporation[31] in contrast to the microwaved based procedure used in this work. Both of these examples however are not hybrid devices since they do not couple existing semiconductor technology with the new organic technology.
The devices investigated in this project are based on hybrid materials which currently is an uncommon base for memristor devices. Hybrid materials have the potential for making a large impact because they combine the electronic properties of semiconductors with the solution processing advantages of organic materials i.e. low temperature processing and large area coverage at very low cost and on lightweight and flexible substrates.

The structure of the devices studied here consists of a layered structure, like the ones outlined above, electrode/organic/semiconductor/electrode. They comprise of two electrodes sandwiching an array of semiconducting nanorods topped with an organic insulating layer. The device is a bipolar switch, so is able to toggle between memory states by applying alternating polarity of potential difference. Unipolar devices differ from this where the memory state can be switched by successive applications of the same or opposite polarities. The

bipolar switching is hypothesised to be a product of interface effects such as a Schottky barrier involving the charging of the nanostructures and the drifting of oxygen vacancies as seen in TiO_2 described earlier.

The devices developed in this study only use solution processing method for fabrication so are simple, quick and low cost to produce. The devices consist of an inorganic semiconducting material coupled with an organic material, in this case zinc oxide (ZnO) and polymethyl-methacrylate (PMMA) respectively. The basic structure of these hybrid devices consist of a vertical stack of thin-films built upon glass substrates with each layer being added or grown. This procedure is based on a hydrothermal method developed by Greene et al[32, 33,34] in combination with a microwave heating method developed by Unalan[35] and then adapted here, as outlined in Appendix 1 and in Chapter 2. This method is advantageous over other methods, such as sputtering based techniques, because it can be done quickly and relatively cheaply, using simple and widely available equipment.

Thesis Aims

The aim of this thesis work is to achieve an advanced understanding in the following;

1. Modification of the nanorod diameter - The hypothesis was that the nanorod diameter could be manipulated by varying the temperature nanocrystal seed layer would be annealed at from 350°C through to 650°C. This hypothesis was based on the work outlined by Greene. It was thought that this diameter change in turn would alter the resistivity, thereby changing the voltage at for switching resistive states. Changing of the surface area to volume ratio can be important since the mobility of defects at surfaces of transition metal oxides has been proposed to be much higher than in the bulk[32]. The electrical switching properties should then be tuned by changing the diameter of the nanorods. In this work the diameter of the nanorods was modified by annealing the zinc seed layer deposited on the ITO. This has previously been shown to give nanorods with wider diameters[32]. It is expected that annealing causes the nanoparticle ZnO seeds to form larger homogeneous (0001) aligned crystal bases, and would then result in nanorods with a larger overall

diameter. The method involved using a furnace that could reach 1200°C, the standard fabrication procedure was adjusted (hotplate at 350°C), to incorporate the furnace. The resulting slides were imaged in an SEM and processed with MATLAB software allowing the average diameters of the nanorods on each sample to be counted. All of this was to investigate the relationship between the annealing step and the resulting geometry of the rods. It is worth noting that lowering the anneal temperature for the zinc acetate layer leads to less ordered nanorods. Even though temperatures of only 150-200°C are needed for seed alignment, higher temperatures promote seed crystallinity and growth (again seen in the work outlined by Greene[33]).

2. Modification of the ZnO surface Stoichiometry - The second goal of this work was to modify the surface stoichiometry of the ZnO nanorods. An O_2 plasma cleaner was used for this purpose. The hypothesis was that the nanorods could be saturated, at least the top layer of them, with additional oxygen to increase the resistance of the device thus making it more suitable for low voltage operation. The aim of employing oxygen saturation was to change the surface composition of the tops of the rods, since after growth the rods are formed tightly together, with only the tops exposed. The presence of extra oxygen on the ZnO crystal lattice could form an oxygen layer[36], for long exposure times. Over 2 minutes, the plasma treatment is assumed to create oxygen rich sites at the ZnO surface[37] (O^-, O^{2-}, OH^-) possibly increasing the series resistance of the device. Alternatively, it is thought that this extra oxygen could dope the II-VI semiconductor with extra electron holes, as such promoting conductivity[38].
3. Fabrication - Improve the fabrication procedure of the devices so as to remove crystallites that occur as part of the nanorod film growth which have the potential to cause short-circuits in the devices.
4. Understand better the chemical composition, crystalline structure and defect structure of the nanorods and crystallites using X-ray diffraction (XRD) and energy-dispersive X-ray spectroscopy (EDX) and examine how these factors might have a role in the structural and electronics properties of the ZnO material.

Chapter 2, Experimental Details

Fabrication of the Devices and the Equipment used

The devices were fabricated using a multi-step procedure based on a solution processing method. Briefly outlined in Appendix 1, the procedure was based on a hydrothermal method developed by Greene et al in 2008 and then combined with a microwave heating method developed by Unalan. The following standard procedure was derived to use as a baseline of manufacture which could then be tested. This is the growth procedure devised after the characterization of the equipment such as the microwave.

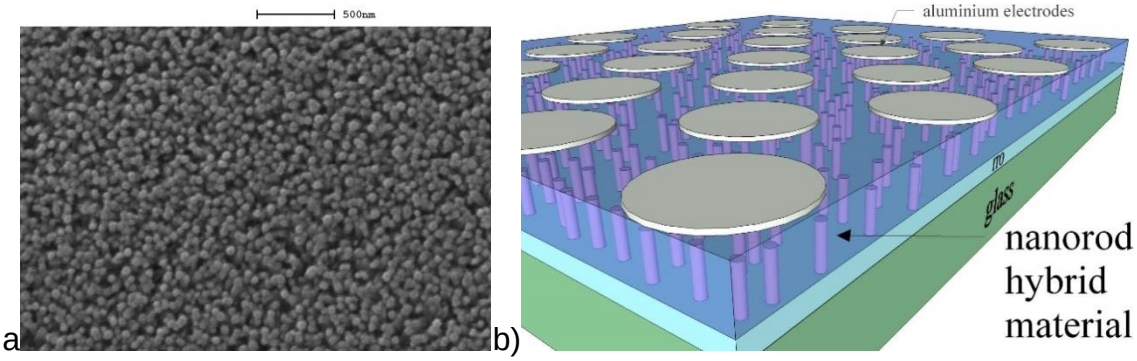

a) b)

Figure 6 – a) Image of nanorods as seen top down on a SEM, b) Representation of typical device structure.

ITO/glass substrates were cut to size when necessary using a diamond scribe. If substrates have been cut to size they must be blown with N_2 gas to remove any glass fragments. These substrates were usually bought in as pre-coated slides, but some uncoated substrates were needed in certain analysis. The substrates were then cleaned using the following procedure using separate beakers for each step

I. 5 minutes in acetone in the sonicator (no heating)
II. 5 minutes in propan-1-ol in the sonicator (no heating)
III. Rinse substrates by dipping them into a beaker containing de-ionized water
IV. Blow dry substrates with gaseous N_2.

The substrates were then seeded with zinc oxide nanocrystals using a zinc acetate dihydrate solution which was annealed to promote the decomposition of the zinc compound to zinc oxide.

I. Spin-coat a 10mM solution of zinc acetate dihydrate, $Zn(CH_3COO)_2.2H_2O$, in propan-1-ol onto the surface of the substrates at 2000 rpm for 30s. (Note**:** The stock solution for this should be made fresh on a weekly basis and stored in the refrigerator)

II. Place the samples onto a hotplate and heat to 350°C for 30 minutes in air. This will align the ZnO nanocrystals with their (0001) plane parallel to the substrate surface.

III. Repeat steps I and ii a further two times to ensure complete and uniform coverage. (i.e. 3 spin and anneals in total.)

IV. Allow the samples to cool in a dry ambient place

The nanorods where then grown on the seeded substrates in a microwave. There were two microwaves used; a regular household model outlined later, and a pressure regulated microwave based in the chemistry department (full method outlined in appendix 1).

I. Make up the solution of equimolar 25mM zinc nitrate hexahydrate, $Zn(NO_3)_2.6H_20$, and hexamethylenetetramine (HMTA) solution in de-ionized water. (Note: dissolve first the zinc nitrate and then the HMTA)

II. Nanophysics Microwave Method: Place substrates into a shallow beaker/crystallizing dish and submerge with 50ml of the nanorod growth solution. Heat in the 900W microwave oven with a weighted lid; first for 30s at 100% power to bring it up to temperature (between 70-80°C measured with an infrared remote thermometer), then for 5 minutes at 20% power to maintain this temperature. Nanorods produced should have a length in the order of 250-350nm (as seen following the method outlined in Greene [32 33]).

Following this nanorod growth step, the substrates were removed from the growth solution and rinsed heavily in deionized water. To prevent potential re-dissolution of the nanorods the substrates were not left in de-ionized water for an extended time. The substrates were then blow dried with nitrogen gas. Following this rinsing step the samples were examined by SEM (if needed). Nanorods on ITO substrates did not need carbon coating prior to SEM examination. The samples were then coated with the organic PMMA layer.

The PMMA had a molecular weight of 120,000 and was supplied by Sigma Aldrich. A solution of 3% by weight PMMA in toluene was prepared and then spun coated onto the grown substrate at 2000rpm for 30s to leave a thin coating (300-400nm) as to cover the nanorods. This was then dried on a hotplate at 180°C for 30 minutes. Following this PMMA layer the top electrode of aluminium was evaporated to make small thin electrodes. The samples set to a height above the aluminium pellet of 20cm resulted in a 150nm layer monitored using a quartz crystal monitor.

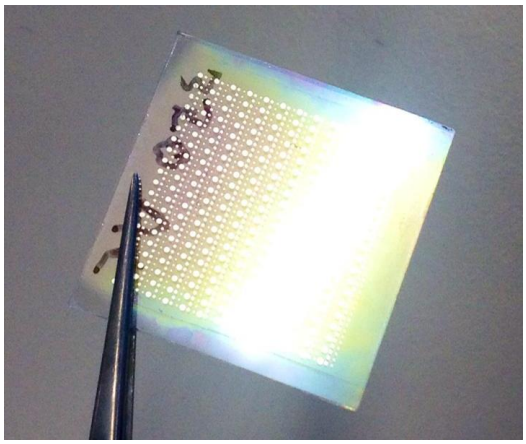

Figure 7 – Image of a finished device, with aluminium electrodes.

The arrays of circles of different size visible on the top surface are individual memristor devices that share a common ITO bottom electrode.

ZnO Nanorod growth

The nanorods were grown using a multi-step procedure based on a solution processing method. Briefly outlined in Appendix 1, the procedure was based on a hydrothermal method developed by Greene et al in 2008 and then combined with a microwave heating method developed by Unalan.

Initially the sample substrates were seeded with zinc acetate dehydrate, $Zn(CH_3COO)_2 \cdot 2H_2O$, dissolved in propan-1-ol. This seed layer is then heated at 350°C to form a zinc oxide nanoparticle layer. The heating also serves to align the nanoparticles to their 0001 plane, parallel to the substrate surface forming a base of growth. This decomposition of the zinc acetate is outlined in the Greene 2008 paper[39] and in a paper by Chih-Cheng Lin[40]

$$Zn(CH_3COO)_2 + 2H_2O \rightarrow Zn(CH_3COO)_2 + 2H_2O \uparrow$$

$$4Zn(CH_3COO)_2 + 2H_2O \rightarrow Zn_4O(CH_3COO)_6 + 2CH_3COOH \uparrow$$

$$Zn_4O(CH_3COO)_6 + 3H_20 \rightarrow 4ZnO + 6CH_3COOH \uparrow$$

$$Zn_4O(CH_3COO)_6 \rightarrow 4ZnO + 3CH_3COCH_3 \uparrow + 3CO_2 \uparrow$$

The thermal decomposition outlined above forms, carbon dioxide (CO_2), acetic acid (CH_3COOH), and acetone (CH_3COCH_3) as by-products.

Following this seeding step, the seeded substrates are then submerged in a solution of zinc nitrate hexahydrate, $Zn(NO_3) \cdot 6H_2O$, and hexamethylenetetramine, $(CH_2)_6N_4$, (HMTA) in deionised water, and then heated to 90°. The following chemistry is one of the more common methods used in synthesising ZnO nanorods[41]

$$(CH_2)_6N_4 + 6H_20 \rightarrow 6HCH0 + 4NH_3$$

$$NH_3 + H_2O \leftrightarrow NH_4^+ + OH^-$$

$$2OH^- + Zn^{2+} \leftrightarrow ZnO + H_20$$

The ammonia (NH_3) produces OH^- ions which drive the crystallisation of the ZnO. This reaction also produces formaldehyde, (HCH0), and water, (H_20), as

by-products. The crystallisation aligns the ZnO perpendicular to the (0001) aligned seeds on the substrate, so the nanorods grow upwards.

Microwave

The microwave used during the growth step needed to be characterised to optimise the growth procedure. The results of this were used to ensure the growth solution and that the slides are at the correct temperature, not boiling, or moving about. The Russell Hobbs RHM2507 Microwave has an input power of 1400W and an output power of 900W[42]. Since the growth solution is water based, the solution can be modelled as ordinary water considering the concentrations of the chemicals involved. 50ml of water was used each time, and the microwave was allowed to cool to ambient temperature between each test.

The first consideration was to find out what temperatures the samples would reach after exposure in the microwave for certain lengths of time on certain power settings. So when the power is set to 100%, when would 80°C be reached? The water temperature was recorded each time it had been heated with and without a lid using an infrared remote thermometer. The following data was produced as a calibration of the equipment.

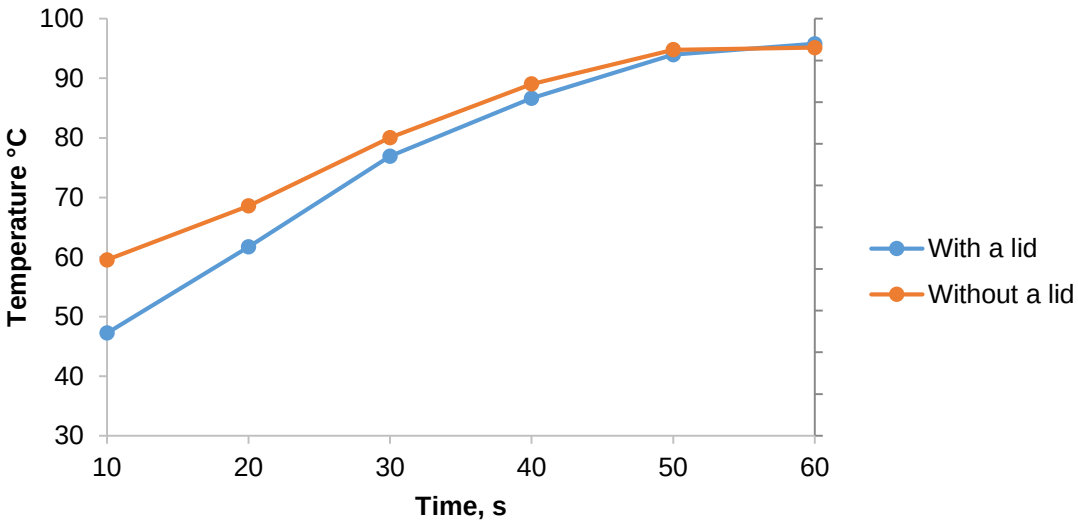

Figure 8 - Average temperature of 50ml water after it has been heated for different times at a fixed 100% power setting.

Knowing that the sample would reach 80°C at around 30-40 seconds with a lid, the next step was to look at what setting would maintain this temperature, by using a lower power setting for a longer amount of time. The goal was to sustain the temperature for 5 minutes.

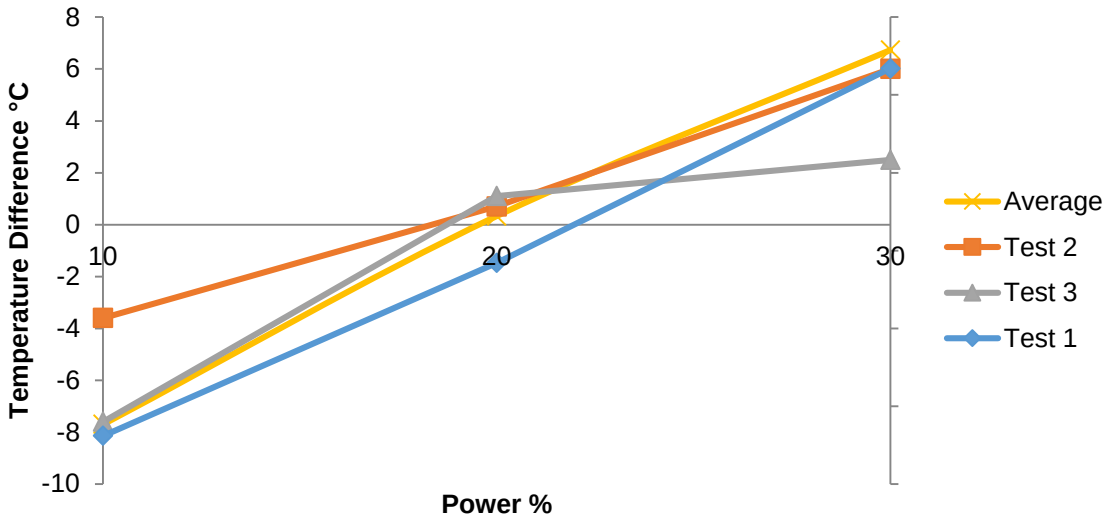

Figure 9 - Difference in temperature after heating sample at 100% for 30s and then continuing to heat the sample for 5 minutes at different power levels.

Using the results recorded in Figure 8, the procedure was amended to allow for the initial heating and the maintaining of the temperature. 30 seconds at 100% power to bring it up to temperature, then 5 minutes at 20% power to maintain this temperature.

Oxygen Plasma Cleaner

A metal evaporator was converted to be used for plasma treatment, typically used for cleaning samples with reactive oxygen plasma to remove contaminants. It uses a high frequency voltage source, set too 350V and 30mA, to excite oxygen gas which is pumped to a low pressure of around $2x10^{-2}$mbar. For long exposure times, over 2 minutes, the plasma treatment is assumed to create oxygen rich sites at the ZnO surface[37] (O^-, O^{2-}, OH^-).

Scanning Electron Microscope

A Cambridge Instruments Stereoscan 360 (S360) Scanning Electron Microscope was used, which could achieve a magnification of up to 40,000 times with clear resolution.

X-Ray Diffraction

A PANalytical Empyrian diffractometer was used, which produces X-Rays corresponding to Copper $K_{\alpha 1}$ emmision at a wavelength (λ) of 1.54056Å. Software used for peak identification was; Highscore Plus, Version (3.0.5) 2012 PANalytical, licensed to the University of Hull. It was used to examine the thin film though a low incident beam, known as Glancing Angle XRF (GAXRF) as it has been shown to be effective in analysing thin films[43].

Energy Dispersive X-ray Analysis

Energy Dispersive X-ray Analysis (or Spectroscopy) is a method of identifying the composition of a sample. Attached to the scanning electron microscope, an Oxford Instruments INCA Chemical Analyser was used to perform a compositional analysis for each sample. With a working distance of 20mm, and magnification set to 3,000x which covered a 30µm x 20µm area. The Extra High Tension (EHT) voltage was set to 5kV and 15kV to take advantage of the beam penetration and examine different depths of the material; 5kV is sufficient to analyse the nanowire layer, whilst 15kV probes into the underlying glass/ITO substrate layers. The count rate was set to 2000 per second and counts were acquired for 100 seconds for each scan, the probe current was used to regulate the count rate, but this is limited as to prevent the filament from blowing. Each sample was examined with 0° tilt on the sample stage.

The Probe Station, Electronic Characterisation of the Devices

A HP 4140B pA Meter / DC Voltage Source was used to take the current readings whilst a voltage was applied to the devices, the voltage was set to 3V and would ramp down and back up between this and -3V in 0.1V steps. The data is typically shown as a hysteresis loop of current vs voltage[44], or it is shown as a log plot of current vs voltage. The data can then be represented as a high or low resistive state (HRS or LRS respectively). This is taken by measuring the gradient between 1 V and -1 V on a current vs voltage hysteresis plot. The station was set to receive an upper current limit of 0.01A to protect the equipment.

Method

Crystallite Characterisation and Growth

Crystallites are unwanted crystal formations that appear on the samples. Varying from 0.1um to 10um in size, it is thought that they could have a significant effect on the switching of the devices. To identify their composition, their structure, which stage of our procedure they come from, and if they affect the electronic properties of our devices, a series of characterisation techniques was used.

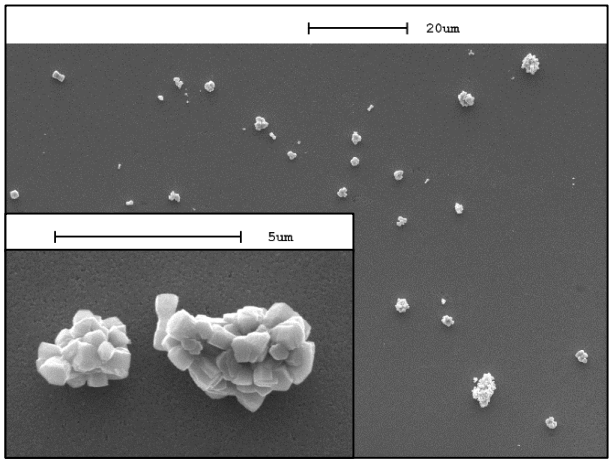

Figure 10 - Typical crystallites found on an early sample at 1k and 7.5k magnification.

Crystallites were found through SEM and it has been observed that they reoccur many times in past samples. This has led them to become a problem since they are relatively large, have an unknown electro physical behaviour, and have an unknown source. The hypothesis was that they are formed in the growth step and that their density and/or their structure are dependent on the time the solution is heated. It is thought that they are formed either on the substrate directly, suspended in the solution, or a combination of both. A preliminary enquiry was undertaken to see if it was possible to produce samples with only crystallites and no nanowires. Using these results to assess the best way to produce further crystallites, a good procedure could allow an investigation into the electro physical properties and see if they are affecting the results, what causes them to form, and what dictates their size.

X-ray diffraction (XRD) patterns were taken of three samples; one sample had the regular method nanorods, the second sample had the growth solution spin coated onto it, and the third had the growth solution rapidly dried onto the

surface by means of the glass substrate being placed onto a hotplate set to an excess of 200°C. All of this was to see if there was any unknown chemistry behind the crystallite formation.

Crystallite Densities

Two glass slides were prepared using the usual cleaning method (outlined in Appendix 1), two beakers containing 50ml of the growth solution were then heated, and the glass slides were not in the solution at this stage. Both solutions were heated at 100% power for 30s to bring them up to a temperature of around 80°C, and then one was heated at 20% for 1 minute and the other was at 20% for 5 minutes to maintain this temperature for these times. These two solutions were quickly spin coated onto the two individual glass slides three times at 2000rpm for 30 seconds and then heated on a hot plate at 150°C to evaporate any residual liquid, with the aim to deposit any crystallites formed in the solution onto the slide. These slides were then carbon coated and stuck to carbon tabs and sample mounts to prepare them for SEM imaging.

Crystallite and Nanorod; Composition and Orientation

Three glass slides were prepared for use in the X-Ray diffractometer, they all had to be cut to size to fit in the sample holders. The sample holders were circular with a diameter of 32.13mm, so the diagonal of the glass slide had to match this diameter. Since the glass slides available were 25.4mm wide and over 70mm long, they had to be cut down to 19.67mm to produce slides to fit in the sample holders. The resultant dimensions of the slides were 25.4mm x 19.7mm. The slides where then cleaned with the usual method of sonication. A base growth solution was then prepared. The first slide, to produce nanorods, underwent the usual seed, anneal and growth steps, using the same growth solution outlined above. The second slide, looking at spin coated crystallites, was spin coated at 2000rpm for 30s with this resultant growth solution three times, after each time heating on a hotplate at 300°C to promote adhesion. The third slide, looking at the solution being dry coated onto the sample, used the same growth solution. By placing the prepared slide on a hotplate set to 300°C and using a pipette, the solution was quickly dried drop after drop onto the slide to build up a crystalline layer.

Surface Size

The hypothesis was that the nanorod resultant diameter could be manipulated by varying the temperature. Nanocrystal seed layer would be annealed at temperatures from 350°C through to 650°C this hypothesis was based on the work outlined by Greene[45].

Four ITO coated glass slides were prepared, using the standard cleaning procedure. Instead of the usual procedure (spin coating and then annealing the slides at 350°C on a hotplate for 30 minutes, and this being repeated 3 times), the objective was to reach higher temperatures; using a furnace fulfilled this objective. Heating the four slides at; 350, 450, 550, and 650°C after each spin coat step, to a total of 3 times. A colour change in the glass to a slight greenish tint was noted, and the 650°C slide warped slightly under the heat. It is doubted that this would have affected the diameter of the rods given the magnitude differences of the warping and expected nanorod diameters, (under 100nm).

After the annealing step, the slides underwent the standard growth procedure. Nanocrystal formations on the sample can be quickly inferred by observing interference patterns when light is reflected across the samples, see Figure 7 on page 20. The samples were then imaged using the SEM; the resulting images were put through a script in MATLAB, Appendix 2.

ZnO Nanorod Surface Stoichiometry

The second goal of this project was to modify the surface stoichiometry of the ZnO nanorods. An O_2 plasma cleaner was used for this purpose. The slides underwent the usual cleaning, seeding, and growth procedure. Following this they were exposed to oxygen plasma in an O_2 cleaning device set to 350V and 30mA, for varying amounts of time. These samples where then imaged under the SEM, and were also studied with XRD, and EDX, to infer if the crystallinity of the nanorods on each sample had indeed been changed, and if the relative compositions of each of the main elements alter; all to verify if oxygen had indeed been added. Finally the electrical properties of the devices were measured, to see if the conductivity had changed. In preparation for XRD, the nanorods were grown on glass slides cut to size (method shown on page 27). A total of six samples were prepared; a control sample, and 4 others that were exposed to O_2 plasma for 1, 5, 10, and 20 minutes.

Chapter 3, Results

Crystallite Characterisation and Growth

Crystallite Densities

The growth of the crystallites was examined by comparing densities for samples prepared with different heating times. Figures 11 and 12 show SEM images of films grown for 1 minute and 5 minutes in the microwave respectively. It can be seen in Figure 11a compared to Figure 12a, that there is a greater density of crystallites on the 5 minute sample. It can also be seen in these figures that the 5 minute sample shows signs of more hexagonal crystallites, whereas the 1 minute sample shows what appears to be a random growth. The following images are what were found on the 1 minute and 5 minute slides, and on a past slide.

a) 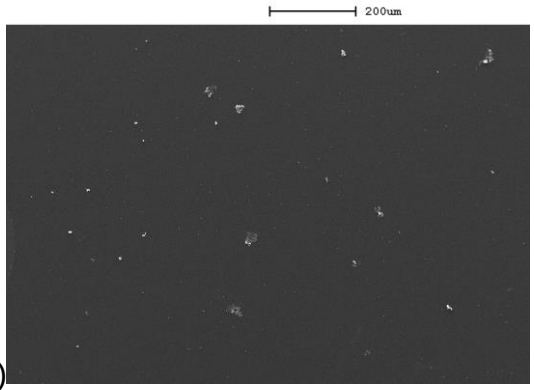

b) 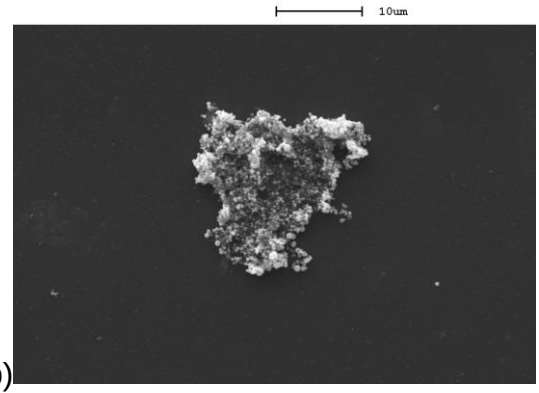

Figure 11 Image of crystallites on the 1 minute sample at a) 100x magnification, and b) 2k magnification.

a) 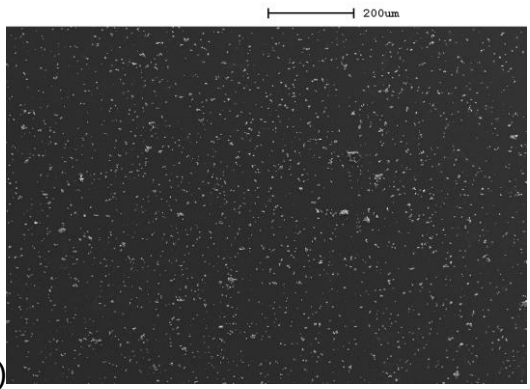

b) 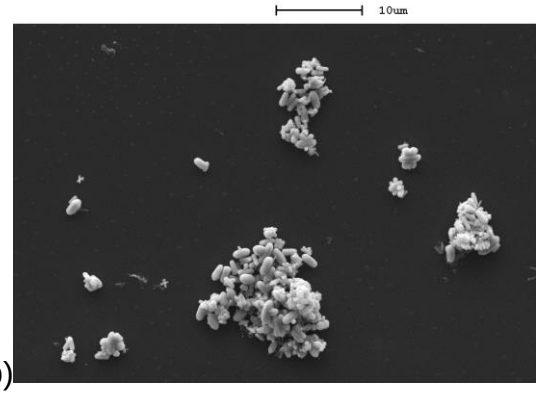

Figure 12 - Image of crystallites on the 5 minute sample at a) 100x magnification, and b) 2k magnification.

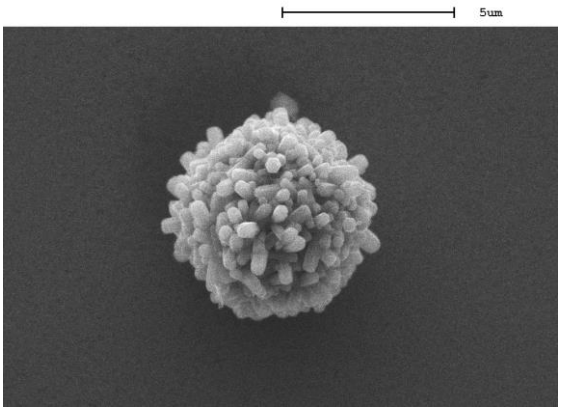

Figure 13 - Image of a crystalline sphere on a past sample. 7.5k magnification

What were not seen in either sample were any crystalline spheres that were seen previously on some initial samples (Figure 13). These initial samples were made to ensure familiarity with the growth procedure and the steps involved with analysing the samples with a SEM. This spherical object was only seen on once slide and its origin is unknown since the sample was prepared with no deviation to the standard growth procedure. This could be evidence that some crystallites are not formed in the solution but on the substrates themselves, perhaps after seeding of smaller crystallite growths formed in the solution and being deposited on the substrate to form these spheres. These spheres seen in Figure 13 are however roughly the same size as the smaller crystallites seen in Figure 12, at roughly 5um, this could counter the hypothesis that smaller crystallites are seeding the formation of these spheres.

Crystallite and Nanorod; Composition and Orientation

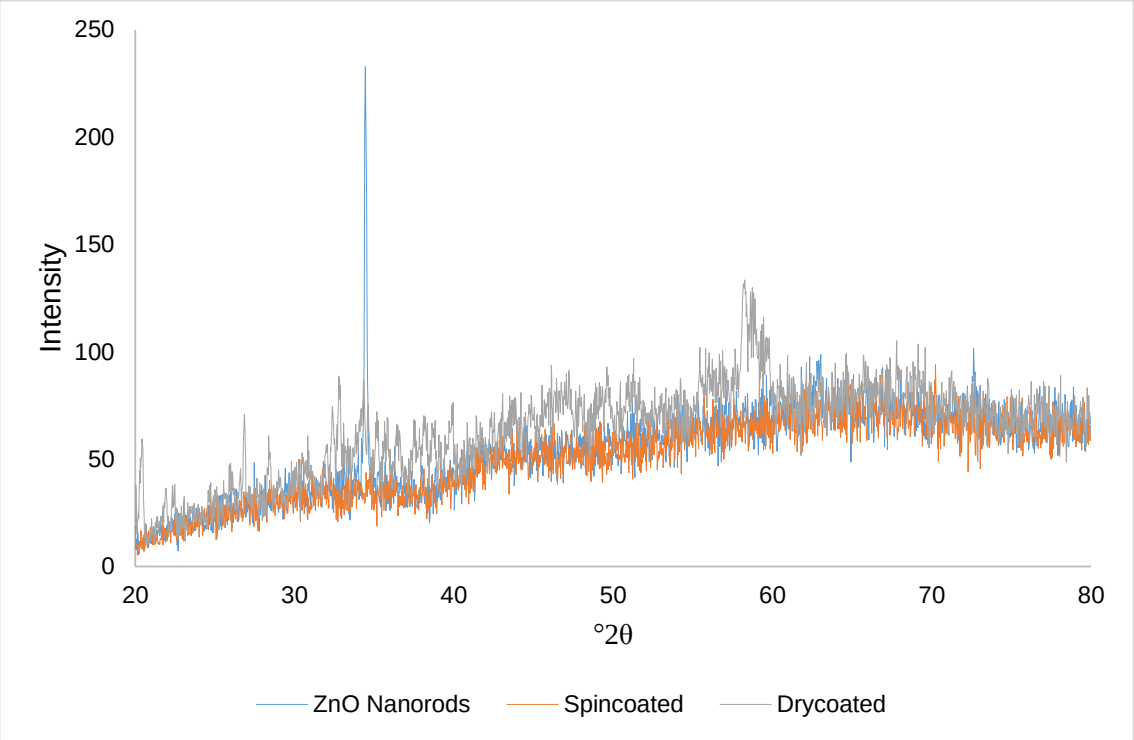

Figure 14 - Thin film XRD of; ZnO nanorods grown onto a substrate, ZnO spincoated crystallites, and ZnO dry coated crystallites. Intensity vs Bragg angle

In Figure 14 the ZnO nanorod curve shows a strong peak at 34.46° corresponding to the wurtzite structure indicating a preferential crystalline alignment that follows the vertical c-axis[48]. The peak at 34.46° is the (002) peak, there are also two other, harder to see, peaks at; 63.03° and at 72.63°, corresponding to a (103) peak and a (004) peak respectively. All of these peaks are L components of ZnO and are consistent with a wurtzite structure[47]. The entire range of peaks typically associated with ZnO cannot be seen in Figure 14 however, the usual peaks observed being; (100), (002), (101), (102), (110), (103), (200), (112), (201), (004), and (202)[47]. Figure 14 shows; (002), (103), and the (004) peaks, the fact other sources usually get the entire range of peaks is because they usually remove the nanorods/wires from the substrate and conduct a powder diffraction[46], the X-Rays are then diffracted through the entire range because of their random orientations in the powder, an example of this peak range is shown below (Figure 15).

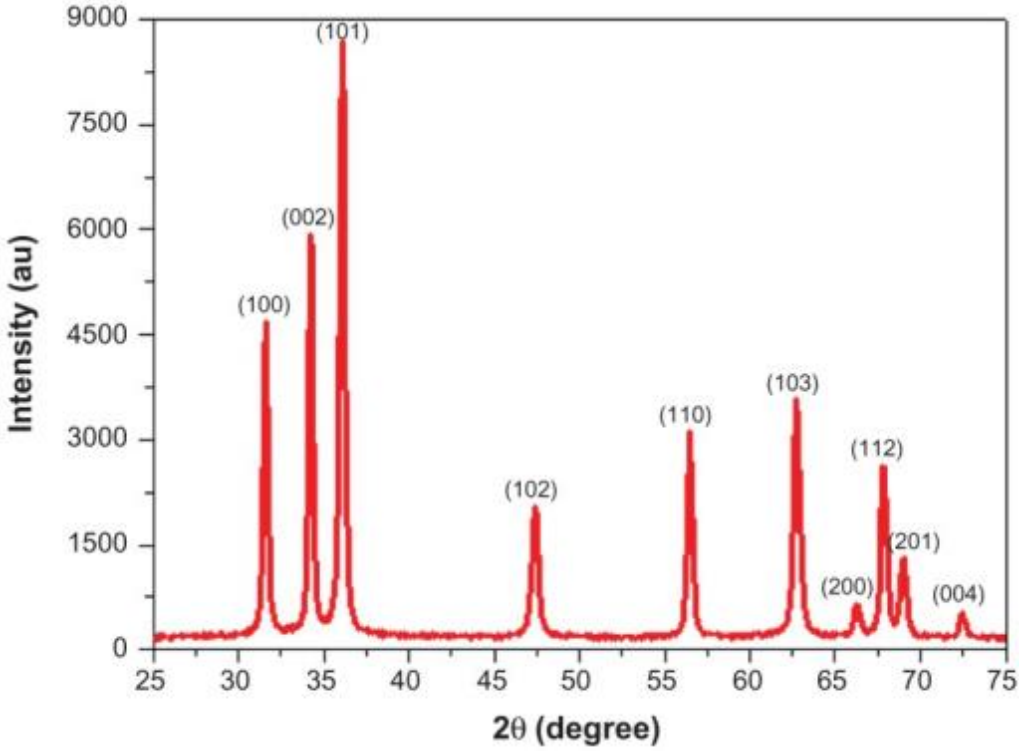

Figure 15 - A typical XRD pattern for ZnO Nanoparticles (from [47])

The samples used for this study however leave the nanorods on the substrate and a thin film XRD is conducted, showing only the L components of the ZnO, as such it shows the preferential alignment of the rods along the c-axis[48], i.e. straight up.

The spin-coated sample curve in Figure 14 shows the amorphous nature of the glass from the slide beneath the sample, however it does not show any characteristic peaks associated with anything related to the growth procedure. The dry-coated curve shows more apparent structure, a peak at roughly 58.5°2θ, however nothing could be identified using the Highscore plus software.

Using the peaks visible in the ZnO curve in Figure 14, the dimensions of the unit cell can be found and then compared to an ideal Hexagonal Close Packed (HCP) structure. The lattice parameters a, b, c, in wurzite structures follow the rule; a = b ≠ c, and can be calculated using the following relationship;

$$\frac{1}{d^2} = \frac{4}{3}\left(\frac{h^2+hk+k^2}{a^2}\right) + \frac{l^2}{c^2}$$

Where; *h*, *k*, and *l*, are miller indices (for (002) *h*=0, *k*=0, *l*=2), *a* and *c* are lattice parameters as outlined above, and *d* is the inter-planar spacing found using Bragg's law*;*

$$n\lambda = 2d \sin\theta$$

Where; n is an integer, λ is the wavelength of the incident X-Rays, and θ is half the 2θ (Bragg angle) value attributed to the main peaks. The inter-planar distances are shown in Table 1;

Table 1 - Resulting Inter-planar distances found by XRD

Bragg Angle °2θ	**Miller indicies (h,k,l)**	**Inter-planarspacing (Å)**
34.463	002	2.600
63.037	103	1.473
72.631	004	1.300

Using these distances, the following can be calculated; lattice parameter *a* = 3.227Å, lattice parameter *c* = 5.201Å, and the packing factor (the *c/a* ratio) equates to 1.611, the ideal c/a ratio for HCP structures being 1.633[49].

Table 2 - A comparison of calculated XRD values with accepted values.

Lattice Parameter	**Calculated Results**	**Accepted Results [20, 50]**
a	3.227Å	3.24981Å
c	5.201Å	5.20653Å
c/a ratio	1.611	1.633

Determination of the Nanorod Diameters

MATLAB

A Matlab code was written to analyse the images from SEM (outlined in appendix 2). With this code, Matlab would compile a list of diameters and the total number of nanorods identified in each image, we then processed it accordingly.

The program was not able to process the image of the sample annealed at 350°C due to issues with contrast and resolution. The following is the nanorod diameters counted in each image. As an early deduction it can be seen that there is a slight growth in diameter as the annealing phase in the procedure reaches higher temperatures; however the current diameter averages show minute changes, possibly due to the skewed nature of the histograms.

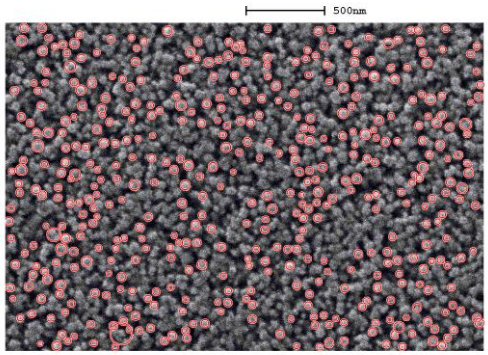

Figure 16 - SEM Image with the seed annealed at 450°C, Sensitivity set to; 0.890, Total count in image of 453.

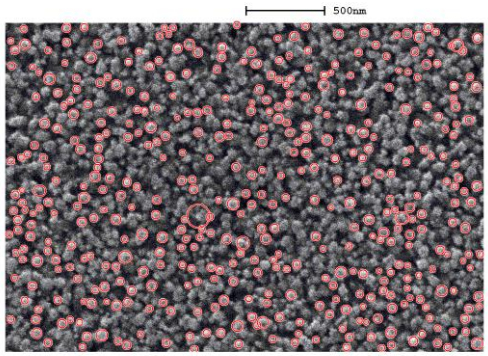

Figure 17 - SEM Image with the seed annealed at 550°C, Sensitivity set to; 0.900, Total count in image of 432.

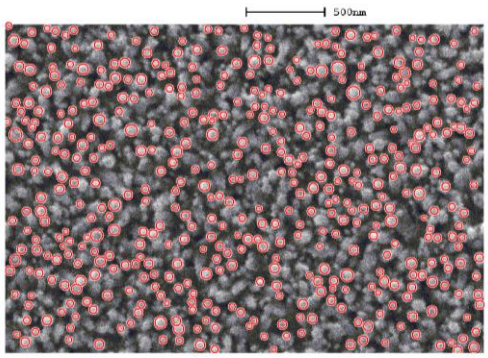

Figure 18 - SEM Image with the seed annealed at 650°C, Sensitivity set to; 0.895, Total count in image of 468.

Using the data from MATLAB in processing the images in; Figure 16, Figure 17, and Figure 18, the following histogram was produced as a direct comparison.

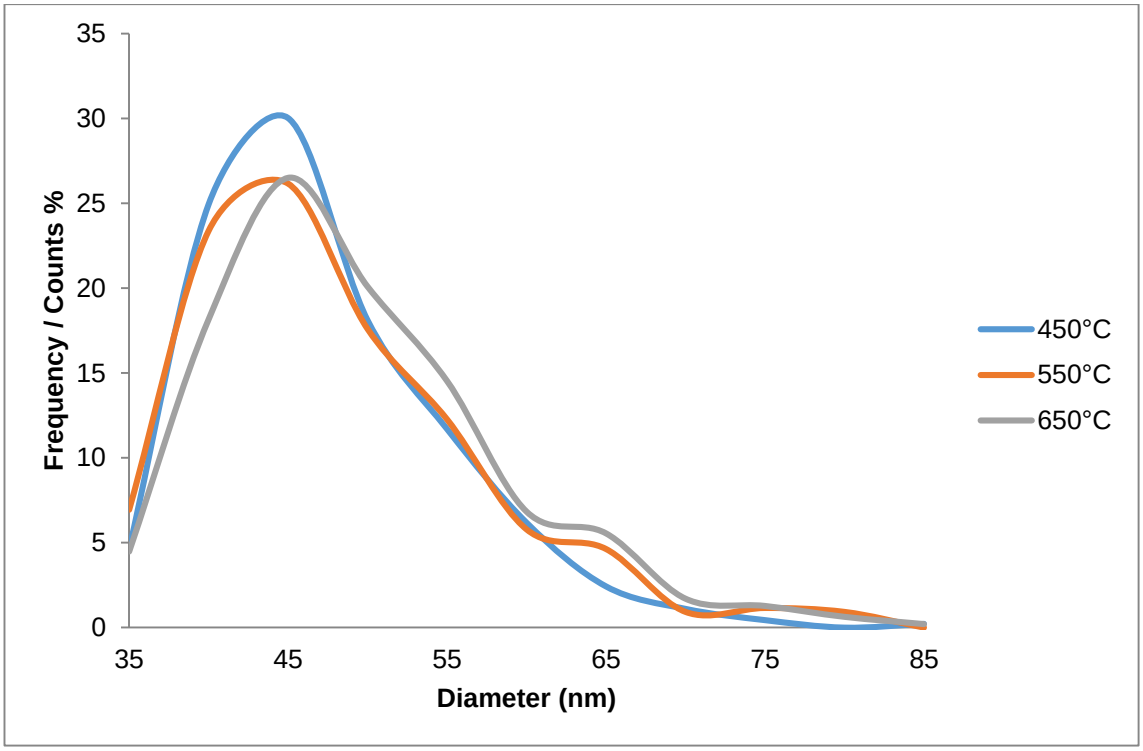

Figure 19 - Ratio of diameters against counts for each annealing temperature

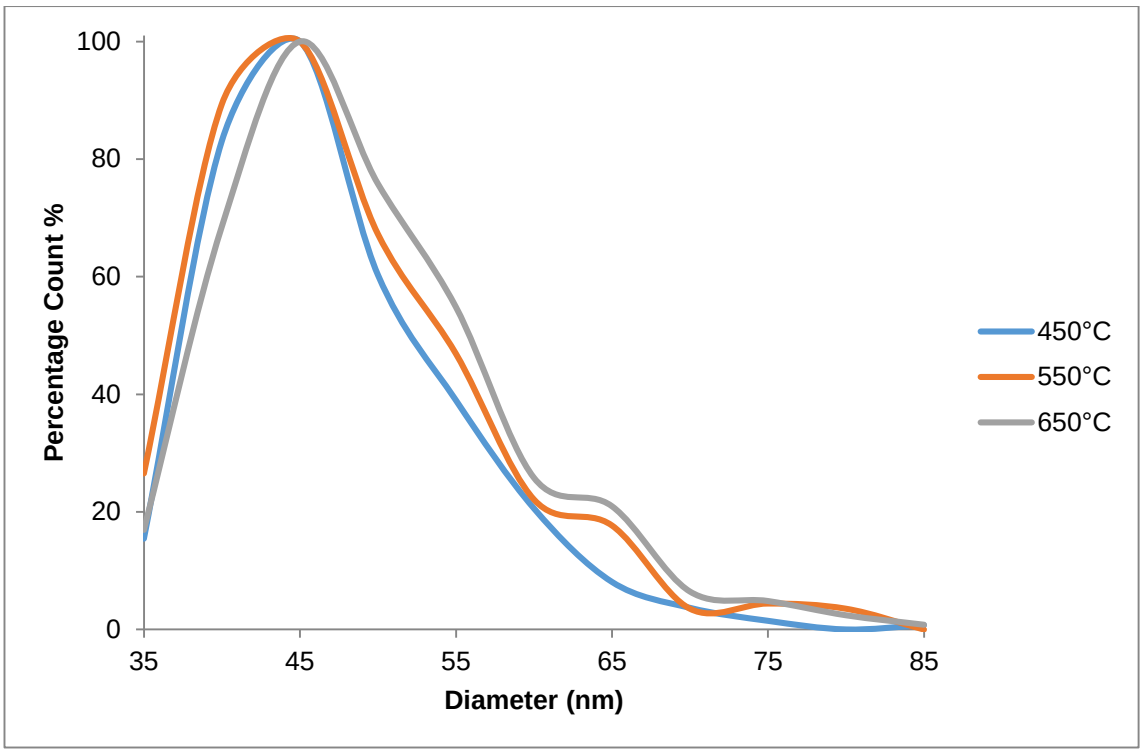

Figure 20 - Percentage of counts normalised against the main peak (at 45nm).

From the above histograms the following diameter averages of the nanorods are shown in Table 3;

Diameters (nm)	450°C	550°C	650°C
Average	44.7	45.5	46.8
Median	42.8	43.3	45.1
Mode	42.8	41.3	44.7

Table 3 - Resulting average nanorod diameter for different annealing temperatures.

Electrical Properties; Current/Voltage Testing.

The current/voltage characteristics were measured using a voltage source and two tungsten probes connected to both the; ITO bottom electrode, and the aluminium top electrode. These voltage/current readings are shown Figure 21.

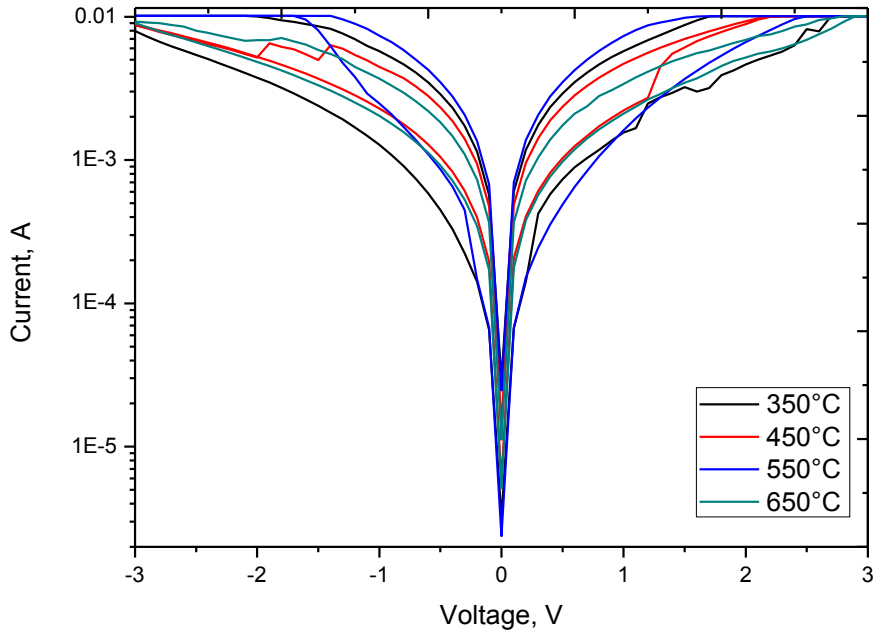

Figure 21 – I/V curves for ZnO/PMMA hybrid memristor devices with different annealing temperature for the seed. Resistive switching observed with the surface composition slides. Current measured when a potential difference of 3 volts to -3volts is applied. Sweeps flow from 3V to -3V and back at 0.1V steps.

Figure 21 shows the resistive switching found on the surface size slides where the zinc acetate seed layer has been annealed at different temperatures with the aim to change the nanorod diameter. The curves drawn in this figure start at 3V and then ramp down to -3V along the lower curves, they return to 3V stepping up the voltage from -3V. The figure above clearly shows no significant difference in the operating current of the devices or with the switching behaviour as the annealing temperature is increased. Although it is not immediately apparent with the SEM images (Appendix 4, Figure 38), ZnO does begin to deform upwards of 600°C - 700°C[51]. It was hypothesised that this deformation, however slight and noticeable, would yield changes in the operating current In Figure 22 below. No significant change in resistance is seen however. Figure 21 no trend in the On/Off ratios of the devices is seen.

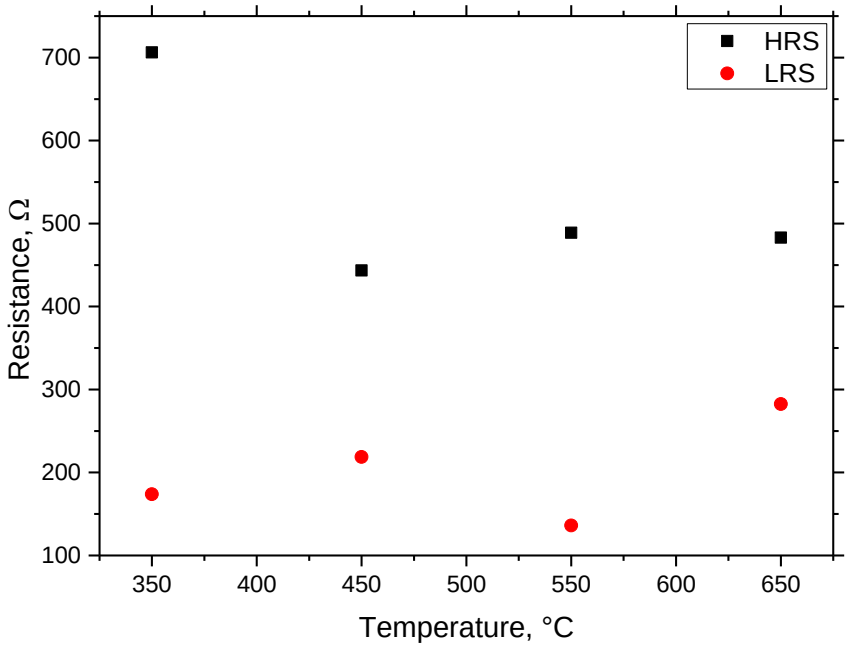

Figure 22 - Resistance of the high and low states versus annealing temperature. HRS high resistive state, LRS low resistive state.

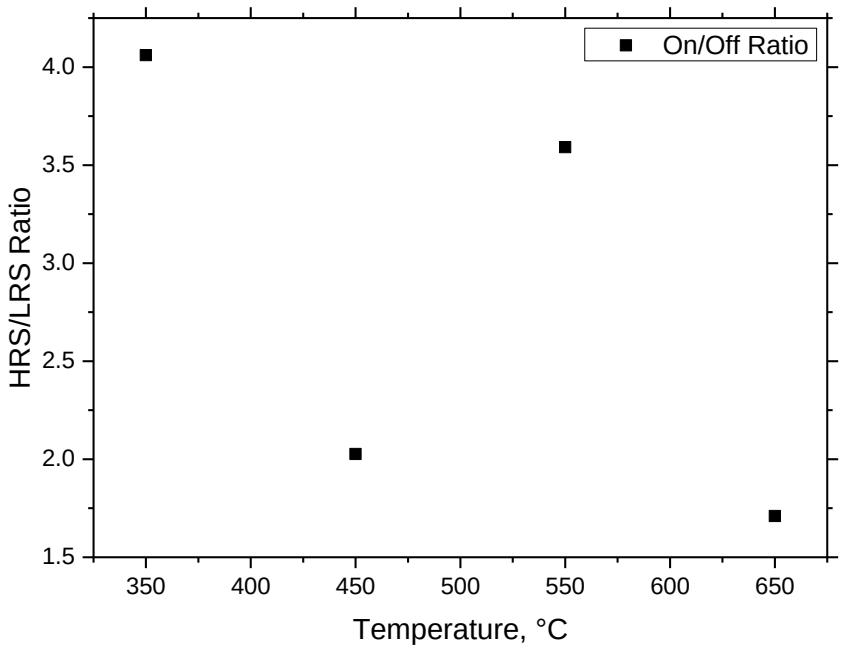

Figure 23 - On/Off ratio for the resistive states against annealing temperature

Surface Composition

Relative Compositions

The following is a study into the effect of O2 plasma exposure on the performance of these devices. These samples underwent the standard annealing and growth procedures, and after SEM and EDX analysis were coated with PMMA and had aluminium electrodes added for electrical testing.

Energy Dispersive X-Ray Analysis

The following is the X-ray analysis (EDX) of the control slide at 15kV; this reveals all the expected elements that are in the sample, namely the ITO electrode layer and the glass substrate. For the analysis of the samples however, a beam current of 5kV was used. This is to minimize the beam penetration and focus the results to the bulk of the nanorods being examined, and not include both layers of the sample and glass substrate underneath.

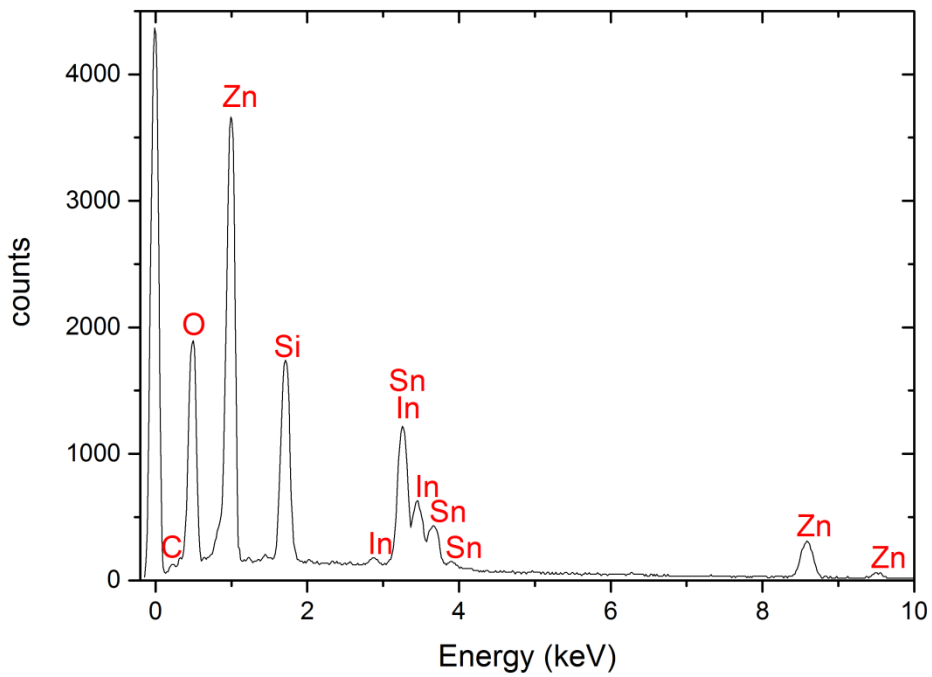

Figure 24 - EDX of the control sample, consisting of a regular ZnO nanorods without oxygen plasma. The EDX is taken at 15kV.

The 15kV scan of the control sample shown in Figure 24 shows that the electron beam is used to probe throughout the entire sample and substrate. Because of this the following can be seen; (from left to right in the graph) A

carbon peak (C), this probably corresponds to any residual HMTA ($C_6H_{12}N_4$), acetic acid (CH_3COOH), acetone (CH_3COCH_3), formaldehyde (HCH0), left over by products from the hydrothermal growth of the nanorods, or possibly from any foreign objects on the sample such as any nanoscale dust build up. The oxygen peak (O) will correspond to four oxides; glass SiO_2, the ITO electrode layer which typically comprises of; In_2O_3 and SnO_2, and of course the ZnO nanorods. The zinc peaks (Zn) are from the same nanorod layer. The magnesium and aluminum peaks (Mg & Al) are relatively small, and are probably impurities in the glass (in this case Al_2O_3 and MgO, see data sheet[52]). The silicon peak (Si) is from the glass and ITO layer. The indium and tin peaks (In & Sn) are from the ITO (indium tin oxide) electrode layer. The peak just above 0keV (located at 0.025keV) is the background emission of X-rays from the sample and equipment caused by the electron beam, this is constant across the samples and was used to normalise the following data.

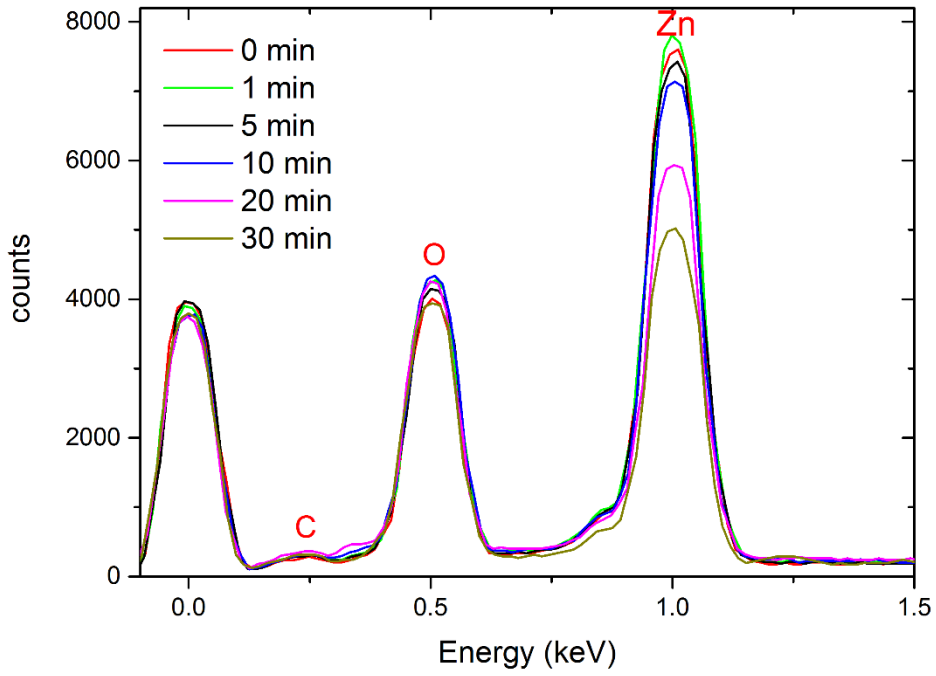

Figure 25 - EDX of all 6 samples, 5kV. As a function of plasma exposure time.

In Figure 25 the five EDX curves of the sample are compared, using 5kV to minimize beam penetration, it can be seen that the background peak is roughly constant throughout the curves and as such this can be used to normalize the data, since the raw data is semi-quantitative. Each of the individual EDX curves

is shown in Appendix 5. Using the data from Appendix 5 the following graphs were produced.

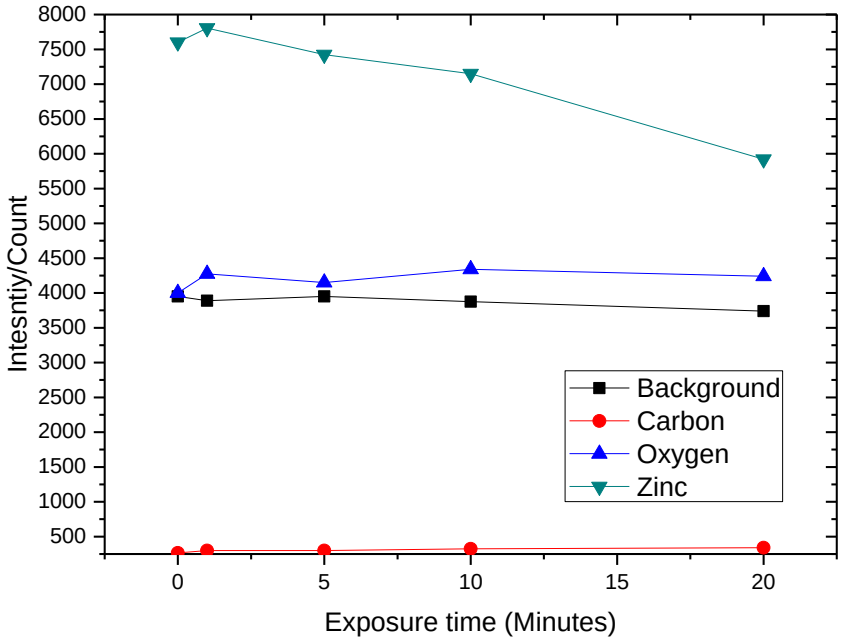

Figure 26 - Peak heights for each element and showing the raw count data from the EDX

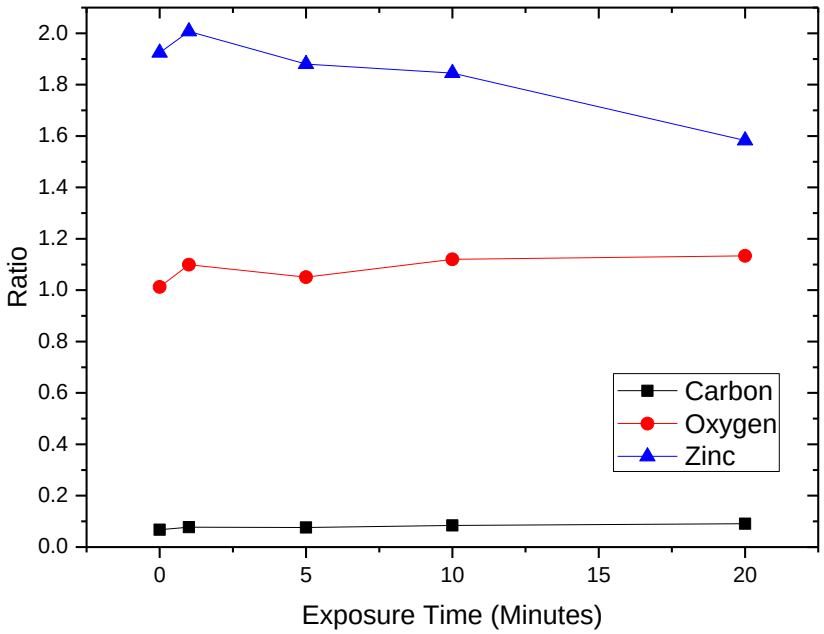

Figure 27 - Peak heights for each element relative to the background peak and showing a clear decline of the zinc relative to the background scatter

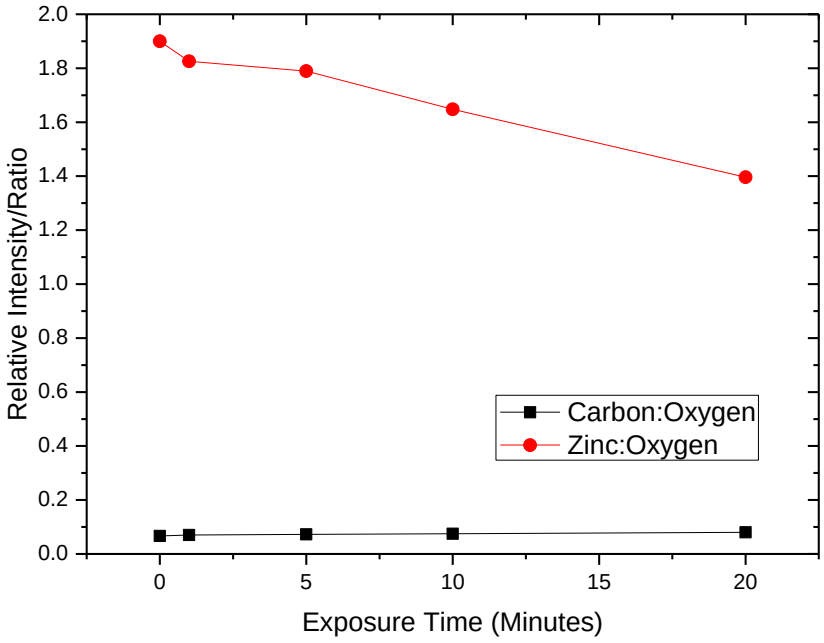

Figure 28 - Element to Oxygen ratios and showing that the zinc:oxygen ratio declines with exposure to O_2 Plasma

Figure 26 shows the peak heights for each element identified in the EDX scans as well as the background peak, since this background peak remains relatively constant; this was used to normalize the data to produce the following relative intensities. A clear decline along the zinc curve can be seen in Figure 27, with a slight incline on the oxygen curve. This decrease in zinc relative intensity has led to an overall increase in the resistance of the devices. The carbon peak, like the background peak, remains relatively constant suggesting something constant across each of the samples suggests the presence of nanoscale dust build-up. Figure 28 is the element to oxygen ratios observed in the data from Figure 26. It shows a clear decrease in the zinc:oxygen ratio whilst the carbon:oxygen ratio remains constant.

X-Ray Diffraction

The following are the XRD patterns for each sample. A clear crystallinity is seen in the samples along the C axis, which indicates that the crystal structure of the sample is pointing upwards with respect to the substrate, strong evidence for the growth of nanorods. Changes in the locations of peaks would correspond to alterations to the crystal structure, something expected from heavy oxygen doping, since any changes in the crystallinity can be inferred from these peak locations. It must be noted that not much can be read from the intensities of each peak since the only way to directly compare intensities is to examine them at the same time with the same beam in the same conditions, something which the equipment was not designed to do. As such the relative intensity across these samples does not necessarily correlate to any change in composition.

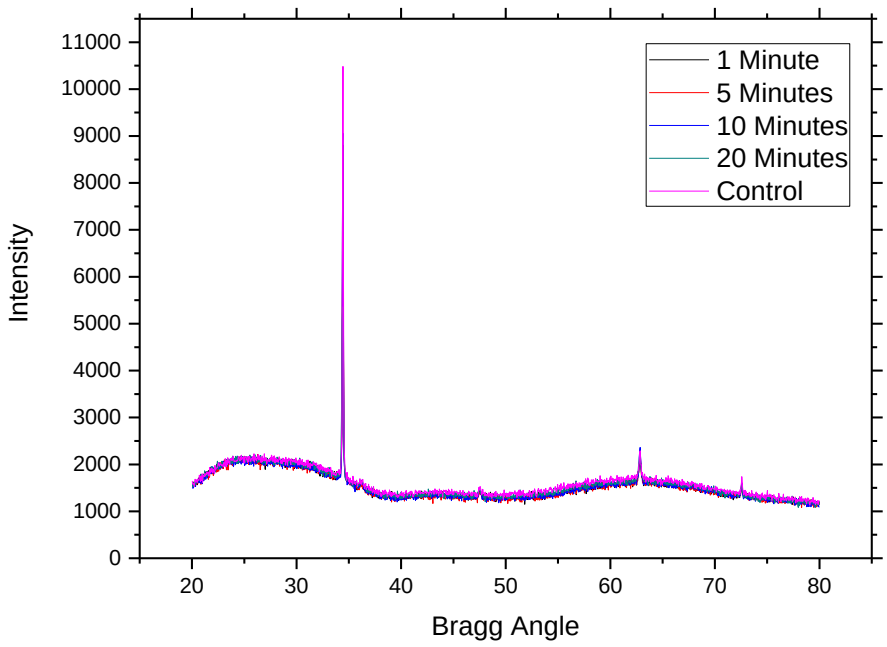

Figure 29 - Thin film X-Ray diffraction patterns of the samples after; 0, 1, 5, 10, & 20 minutes of O_2 plasma exposure. Intensity vs Bragg angle

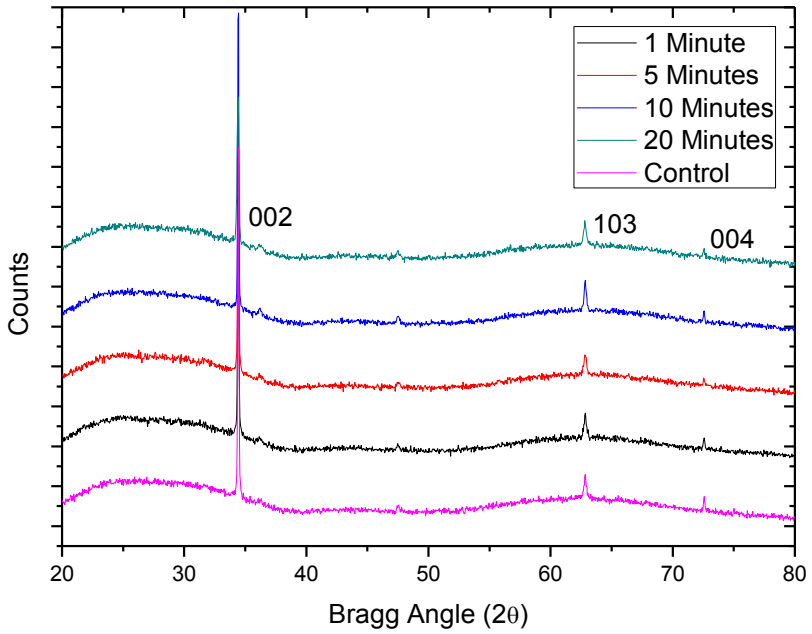

Figure 30 - A comparison of peak positions in the patterns from Figure 29. The peak at 34.46° is the 002 peak, at 63.03° the 103 peak, and at 72.63° the 004 peak. As a function of plasma exposure time.

The above XRD plots were used to calculate the planar spacing between each lattice and as such the lattice parameters and axial ratio of each sample. So using the curves from Figure 30, the lattice parameters of the crystalline structures present on each sample can be found, as well as their c/a ratios. The full width at half maximum for each of the planar peaks was also examined.

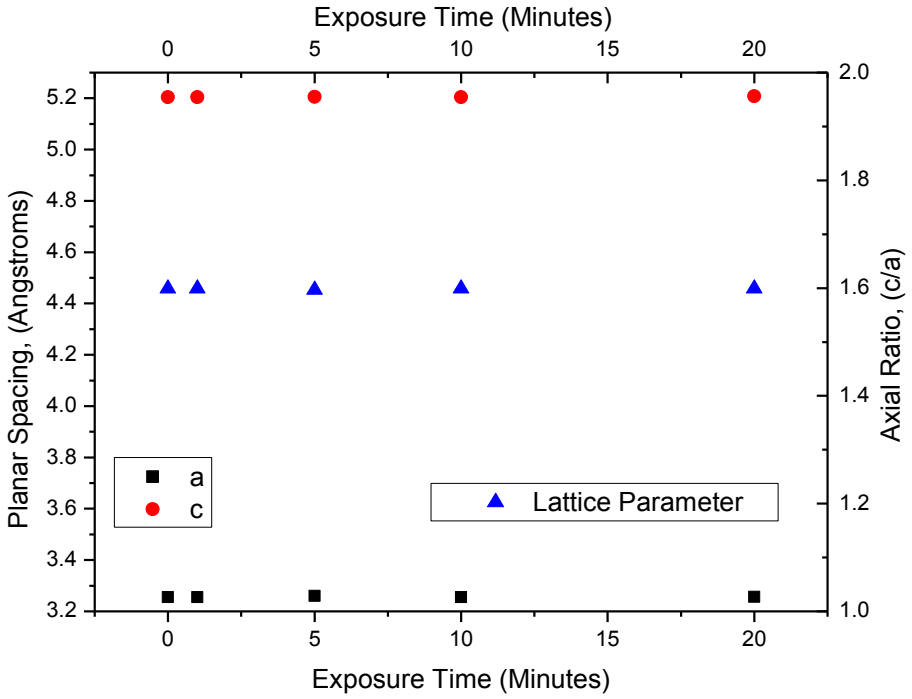

Figure 31 – Planar Spacing,a (■) & c(●) and the a/c ratio (▲) versus O_2 plasma exposure time.

In Figure 31 there is very little difference that can be seen between the control (no exposure) and the sample after varying times of exposure. (See Appendix 6 for all the data derived from the XRD plasma samples)

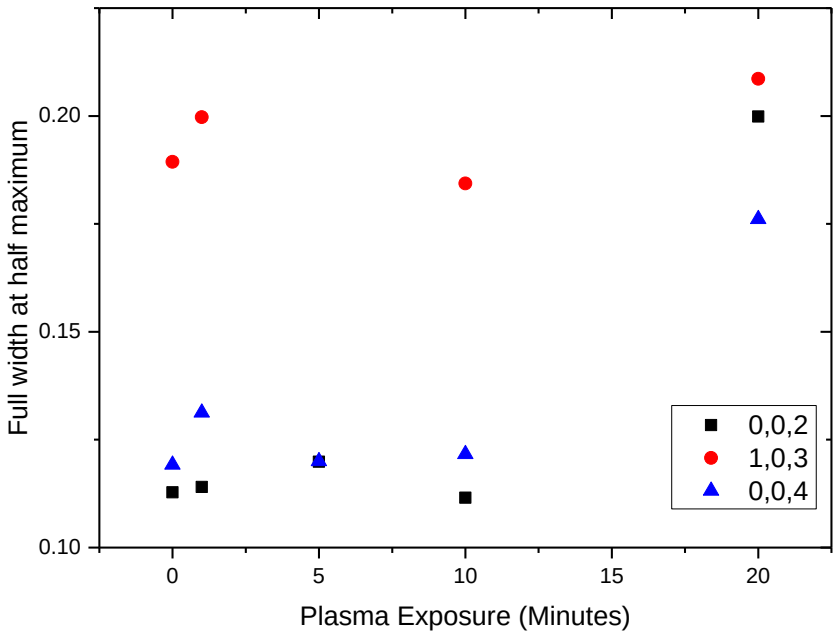

Figure 32 - Full width at half maximum of the 3 main peaks versus O2 plasma exposure.

The equipment used was ideally suited for powder x-ray diffraction. Since the samples are thin films, this can lead to the peaks at lower angles of 2θ to be moved and broadened, and as such is less reliable[53]. It can also lead to the background curve intensifying. The (004) peak is located at 72.63° and is less affected by this factor. This should be taken into account when looking at the full widths at half maximum of each of the peaks characterised above in Figure 32. Taking the above information into account and looking at the (004) peak, the FWHM is seen to increase suggesting that the peak is broadening with plasma exposure, indicating a decrease in crystallinity. Ultimately this must be repeated with the proper equipment to verify this conclusion.

Electrical Properties; Current/Voltage Testing.

The current/voltage characteristics are measured using a voltage source and two tungsten probes connected to both the; ITO bottom electrode, and the aluminium top electrode. These voltage/current readings are shown in Figure 33.

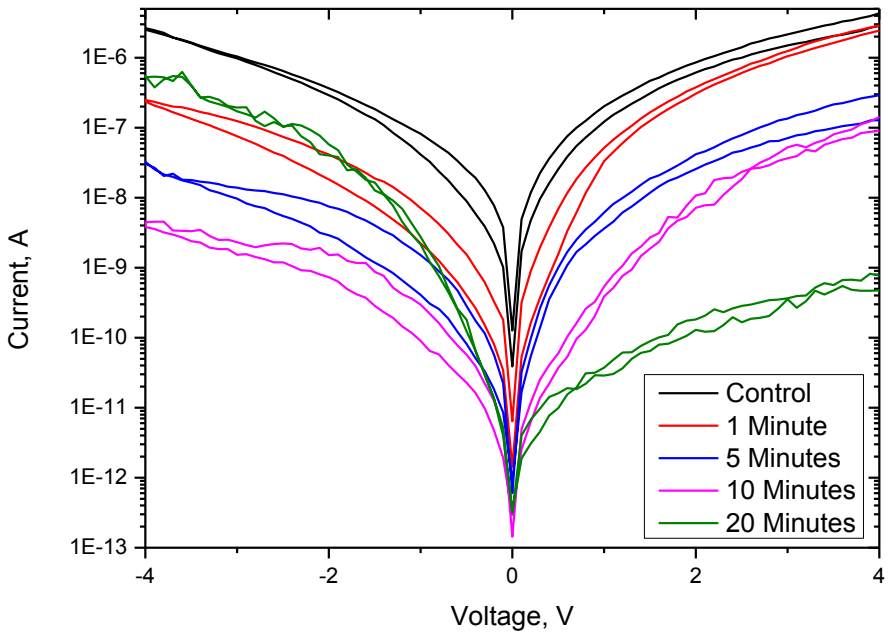

Figure 33 – I/V curves for devices with differing oxygen plasma exposure times showing an increase in the overall device resistance in both the on and off states for increases in plamsa exposure. Sweeps flow from 3V to -3V and back at 0.1V steps.

Figure 33 shows the resistive switching found on the surface composition slides that were exposed to O_2 plasma for times between 0 minutes (control) to 20 minutes. A clear reduction in the operating current of the devices can be seen as the time under plasma exposure is increased, however with the 20 minute device an asymmetrical curve is apparent, this was seen on multiple 20 minute devices. This asymmetry could be accounted by Figure 48 where a slight misalignment of the nanorods is apparent, in comparison to the 10 minute sample, Figure 47, this misalignment has also lead to deformed nanorods which don't show the typical hexagonal structure. This asymmetry of the 20 minute devices' I/V curve above could be a result of a device that does not return to its original resistive state. It may have varying depths of the PMMA layer and may not be producing as many conducting filaments.

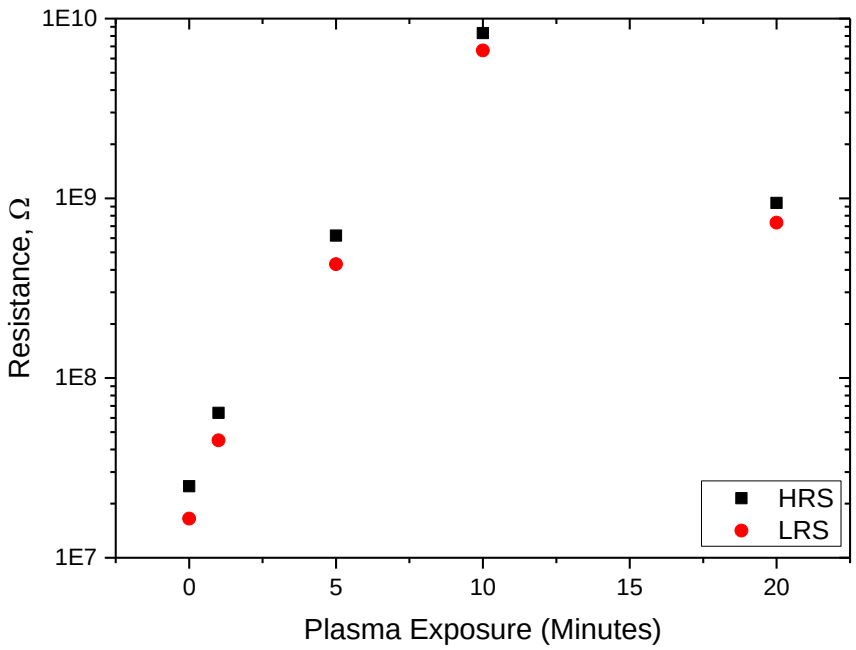

Figure 34 - Resistance of the high and low states versus oxygen plasma exposure time. HRS high resistive state, LRS low resistive state.

In Figure 34 a clear increase of the resistance is seen in both the high and low resistive states of the devices tested above. Again, as with

Figure *33*, it can be seen that the 20 minute plasma defies this trend. This may be due to the deformation mentioned earlier. This decrease in resistance could

also be due to a thinner PMMA polymer layer, a fault during manufacture rather than an inherent property of this sample being treated

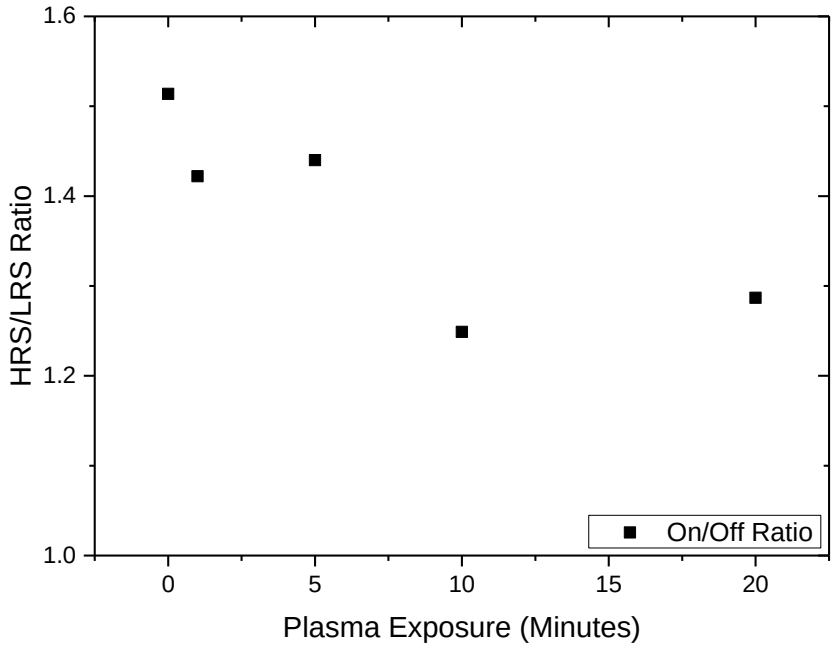

Figure 35 - On/Off ratio for the resistive states against plasma exposure.

In Figure 35, a slight decrease in the On/Off ratio is seen in the devices from above, with increasing the time that the sample is exposed to oxygen plasma. Again, as stated with the previous figures, the 20 minute sample slightly contradicts this trend. Further testing should be conducted to verify this contradiction.

Chapter 4, Discussion

Through the work examining the growth of crystallites it was found from results shown in both Figure 11 and Figure 12 that crystallites are formed in the solution, but possibly also on the substrate; that their density and structure is proportional to time heated, as expected, and that they can be deposited onto slides using a spin coating method. From this work and that seen in papers[54] the growth procedure was amended to heat only the solution for no longer than 5 minutes to minimise crystallite growth. This procedure was then used as the basis for the rest of the work. It was then attempted to examine the crystallite formations through XRD. Looking at Figure 14 the ZnO structure peak at 34.4° is clearly visible in the data. With the spin and dry coated curves in the same figure, the most likely problem is that of crystallite density. The above procedure should be repeated with the aim to achieve higher densities and then it should be possible to measure the lattice structure of the sample using XRD. XRD is a common approach for examining ZnO based structures since they have a well understood composition and stoichiometry. In Saleem's paper[55], a clear XRD spectrum can be seen showing C-axis growth identified by a strong (002) peak at 34.34°2θ suggesting a wurzite structure. This agrees with these investigations above and allows the calculation of the lattice parameters of the ZnO thin film. The lattice parameters found were *a* = 3.227Å, *c* = 5.201Å, and the packing factor (the *c/a* ratio) equating to 1.611 (all from Table 2).

In the work concerned with increasing the nanorod diameters, the initial analysis of the SEM images using MATLAB shows that there is not a significant increase in the nanorod diameters using this method. This agrees with the I-V measurements made on the devices which also showed no significant changes in the current magnitude and switching voltages which also remained constant at around ±1.5V. I-V measurements shown in Figure 22 indicate no statistically significant change in the High or Low resistive states of the devices, despite the original hypothesis. From these results it is suggested that changing the nanorod diameter using this approach is not feasible. This however contrasts with other systems which do show good control of the nanorod diameter throughout changing the size of the seed. In work conducted by C.J.Ward[56] a two-step method in seed meditated growth of gold nanorods is seen, this method could be examined for continuing work in this area involving ZnO

nanorods. However work outlined by Greene[33] shows a good alignment of ZnO nanorods when zinc acetate seeds are deposited on the surface and decomposed at 350°C. At lower temperatures it is suggested in the paper that the nanorods appear misaligned and below 100°C alignment fails completely since the seeds dissolve in the growth solution. One idea is that once the zinc acetate has fully decomposed (seen to happen in the Greene paper at 350°C) then no further changes occur to the seed layer regardless of treatment temperature. As a summary, it may not be possible to change the seed after certain temperatures with existing method of seeding since the full decomposition of the zinc acetate leads to no more useable material left to form large area seeds. One idea is to continue adding seed solution to maintain a constant supply of decomposable material

The work in changing the surface stoichiometry to increase the resistance of the devices was successful. The experiment showed that there is an increase in the resistance of the samples exposed to oxygen plasma as seen in Figure 33. The devices showed signs of switching at around -1.5V to -2V, however this was asymmetrical most likely due to greater migration of oxygen vacancies in the negative direction. These devices did not show similar signs in the positive potential. So whilst a clear correlation was seen between exposure and resistance, this work would need to be continued, perhaps repeating with other oxygen rich environments such as; a furnace with an O_2 atmosphere, or Ultra Violet (UV) ozone treatment would be an interesting path for future investigations. Concerning UV ozone treatment it is necessary to account for the UV absorption properties of ZnO[57]. These adsorption properties would probably favour this treatment. In Faber's work[19], enhanced switching performance of ZnO nanoparticle layers and an overall improvement of device performance is seen. Faber's paper does only investigate oxygen exposures of 0 seconds to 240 seconds (4 minutes) whereas the experiments here investigated up to 20 minutes with a clear increase of device resistance.

Chapter 5, Conclusion

This thesis work was aimed at improving the fabrication and electronic switching properties of hybrid memristor devices consisting of vertically aligned semiconducting ZnO nanorods embedded within an organic polymer (PMMA) matrix. The work is important for two main reasons. Firstly, little is known about the switching mechanism in the hybrid devices. Other investigations in the group were aimed at understanding the electronic transport and switching mechanisms but before these could be carried out it was necessary to develop a strategy for making devices with a high degree of quality control. In particular it is important to control better the growth of the nanorods so as to guarantee that no short circuits are present in the devices cause by unwanted growth of crystallites which sometimes grow alongside the nanorods. The second main reason for the work is that the nanorod hybrid devices have poor resistance on/off ratios. Larger resistance on/off ratio are required because the devices must have two clear states of operation to be a realistic candidate for a binary device. With a larger on/off ratio there is less chance of the two states crossing.

The first goal of the thesis work was to improve the fabrication process by removing unwanted ZnO crystallites that sometimes form during the nanorod growth procedure and which could cause undesirable short-circuits in the devices. The approach here was to examine whether the crystalline structure of the nanorods and crystallites was different as this could provide reasons for why the crystallites might be forming. It was found that the crystallites form in the growth step of the fabrication procedure, with a probable origin relating to impurities in the solution. After this work it was ensured that the solution was made in a clean environment with deionised water rated at a value of anything above 15MΩ. The time that the solution is heated was limited, with a maximum time of 5 minutes to inhibit growth of larger crystallites. It was not possible in this investigation to identify the sole source of the crystallites. It is probable that they are formed on the substrate, in gaps within the seed layer. Low incidence X-ray diffraction thin-film measurements proved to be a quick and reliable way to confirm nanorod alignment and growth along the C axis but was not sensitive enough to detect any deformities in the bulk lattice structure, nor was it sensitive enough to infer the presence of crystallites or measure their lattice structure since they were not concentrated in high enough densities on the sample.

The second goal of the thesis was to improve the resistance on/off ratio in the memristors by modifying the ZnO surface stoichiometry. The nanorod high surface area to volume ratio is expected to be important in switching since it has been shown that the mobility of defects at surfaces of transition metal oxides is much higher than in the bulk. Annealing the nanocrystal seed layer at differing temperatures yielded no notable difference in the device performance. This was unexpected but most likely due to there being no significant increase in the nanorod diameter. Possibly heating the substrates in different environments such as pure nitrogen would yield better results. Another route would be to increase the concentration of zinc acetate used in the seed solution, this would lead to more material being available to enable the growth of larger seeds. It could however result in a higher density of nanorods rather than larger diameters. The results with oxygen plasma treatment show that exposure of the nanorods to an oxygen plasma can be used to increase the resistance of the high and low states (HRS/LRS) of the devices. Energy dispersive X-ray (EDX) spectroscopy results indicated that a likely cause of this increase is an increased amount of oxygen content in the nanorod layer, producing more stoichiometric ZnO.

Future Work.

Following on from this work, there are a few avenues that could be explored in future work;

- Identification of exactly how and when crystallites are formed. i.e. do they form in the solution first and then deposit or do they grow directly on the surface
- Use different techniques to grow nanorods of different diameters (e.g. using nanopore templates of different sized)
- Repeating the compositional analysis of the plasma treated samples with an X-ray Diffractometer specifically designed to measure thin films. As well as a further study into measuring the electrical behaviour observed after treatment in other oxygen rich environments.

Overall, the general aim of the project would remain the same; that is to develop a cheap, efficient, quick way of making zinc oxide based memristor devices.

Appendices and References

Appendix 1 - Standard Growth Procedure for ZnO Nanorods, the preparation method:

This is the growth procedure devised after the characterization of the equipment.

1. **Cut ITO substrates** (if necessary) using a diamond scribe, if substrates have been cut to size they must be blown with N_2 gas to remove any glass fragments.
2. **Clean the substrates** using the following procedure (use separate beakers for each step)
    V. 5 minutes in acetone in the sonicator (no heating)
    VI. 5 minutes in propan-1-ol in the sonicator (no heating)
    VII. Rinse substrates by dipping them into a beaker containing de-ionized water
    VIII. Blow dry substrates with gaseous N_2.
3. **Seed the substrates**:
    V. Spin-coat a 10mM solution of **zinc acetate dihydrate**, $Zn(CH_3COO)_2.2H_2O$, in propan-1-ol onto the surface of the substrates at 2000 rpm for 30s. (**Note:** The stock solution for this should be made fresh on a weekly basis and stored in the refrigerator)
    VI. Place the samples onto a hotplate and heat to 350°C for 30 minutes. This will align the ZnO nanocrystals with their (0001) plane parallel to the substrate surface.

VII. Repeat steps I and ii a further two times to ensure complete and uniform coverage. (i.e. 3 spin and anneals in total.)

VIII. Allow the samples to cool in a dry ambient place (not on plastic)

4. **Nanorod Growth:**

III. Make up the solution of equimolar 25mM **zinc nitrate hexahydrate**, $Zn(NO_3)_2.6H_20$, and **hexamethylenetetramine** (HMTA) solution in de-ionized water. (**Note:** dissolve first the zinc nitrate and then the HMTA)

IV. **Nanophysics Microwave Method**: Place substrates into a shallow beaker/crystallizing dish and submerge with 50ml of the nanorod growth solution. Heat in the 900 W microwave oven with a weighted lid; first for 30s at 100% power to bring it up to temperature (between 70-80°C), then for 5 minutes at 20% power to maintain this temperature. Nanorods produced should have a length in the order of 250-350nm.

V. **Chemistry Microwave Method**: Place substrates vertically into vials and add 20ml of the nanorod growth solution to each vial. Seal the vial to control the pressure and temperature. Select a ramping time of 30 min with a maximum power of 100W to reach 80°C. Maintain temperature for another 30 min with maximum power of 100W. Nanorod lengths should be about 600 nm.

5. Following nanorod growth, remove substrates from growth solution immediately and rinse heavily in deionized water (Rob is looking into using the sonicator for this step, 3 minutes in propan-1-ol without heating). To prevent potential re-dissolution of the nanorods do not leave the substrates in de-ionized water for extended time. Blow dry with nitrogen gas.
6. SEM (if needed). **Note:** nanorods on ITO do not need carbon coating.
7. **PMMA** layer: Use PMMA molecular weight 120,000 by Gel Permeation Chromatography (GPC) (Sigma Aldrich). Dissolve **3%**

by weight in toluene. Spin coat onto the grown substrates at 2000rpm for 30s, then leave to dry on a hotplate at 180°C for 30 minutes.

8. Aluminium evaporation. Use Al pellet with a height above the material set to 20 cm. This results in a 150nm layer. (Or use quartz crystal monitor).
9. Store samples in a vacuum desiccator.

Appendix 2 - The script used in MATLAB. Using inbuilt functions

Open the image

imagename = imread('imagename.bmp');

imshow(imagename)

Measuring tool

d = imdistline;

Delete tool

delete(d);

To find circles

[centers, radii] = imfindcircles(imagename,[# #],'ObjectPolarity','bright','Sensitivity',0.9)

This will list the centers x,y coordinates, and the radii values in pixels

The range of radii it will try to detect here is *[10 30] at [# #]*

The polarity of the object can either be *'bright'* or *'dark'*

The sensitivity can be increased or decreased to fine tune the search, a range of *0.850* to *0.950* is good to try. The sensitivity range is *0.000* to *1.000.* We vary the sensitivity to match a representative portion of the image.

A secondary function to search, add the following in the above bracket string

, 'method', 'twostage'

To find out the number of circles you have found

length(centers)

To highlight the circles in the image

h = viscircles(centers,radii);

To delete the highlight

delete(h);

To print the centers and the radius together so you can copy and paste into notepad

[centers, radii]

Appendix 3 – SEM images of the surface size slides.

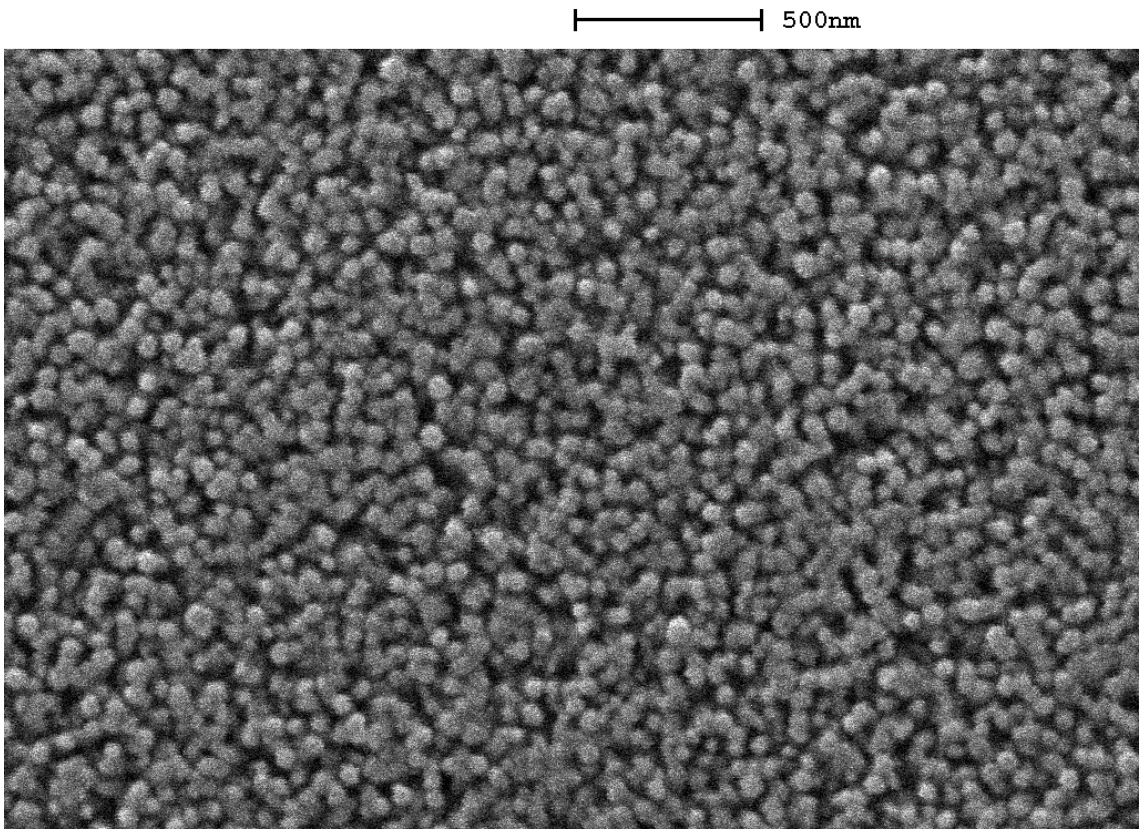

Figure 36 - SEM Image with the seed annealed at 450°C, 40k magnification.

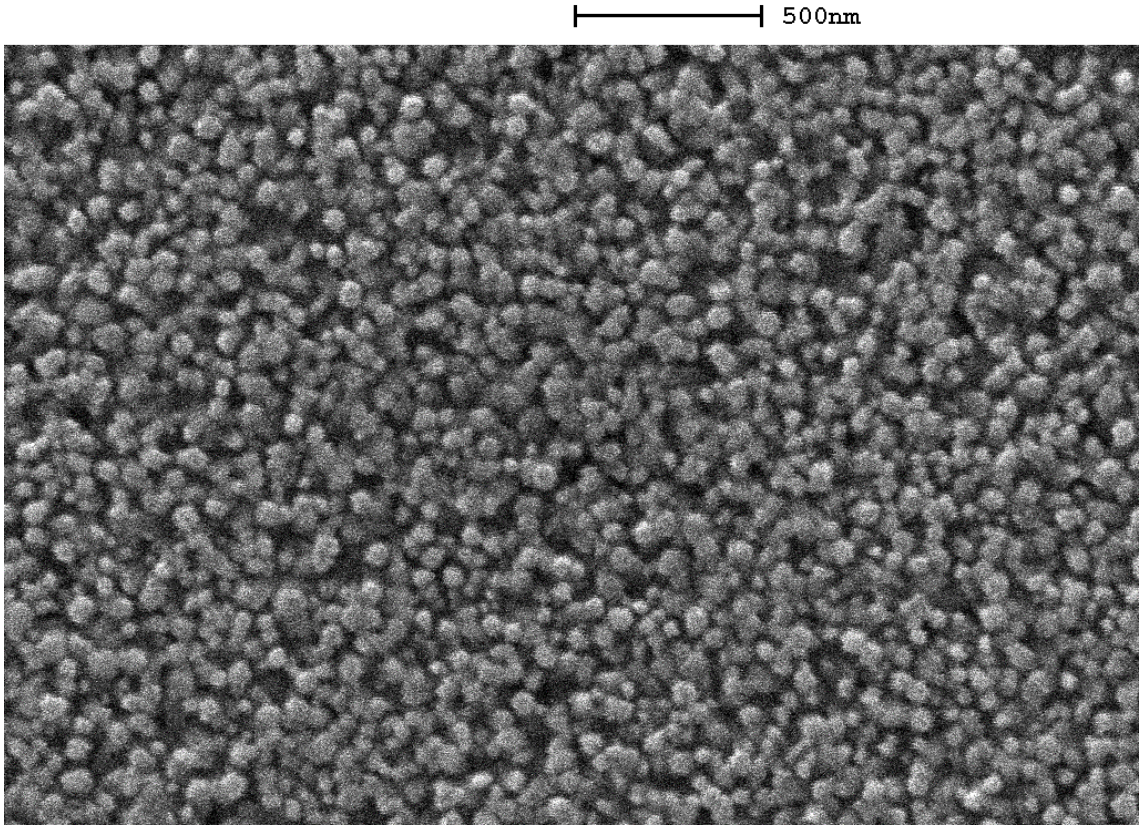

Figure 37 - SEM Image with the seed annealed at 550°C, 40k magnification.

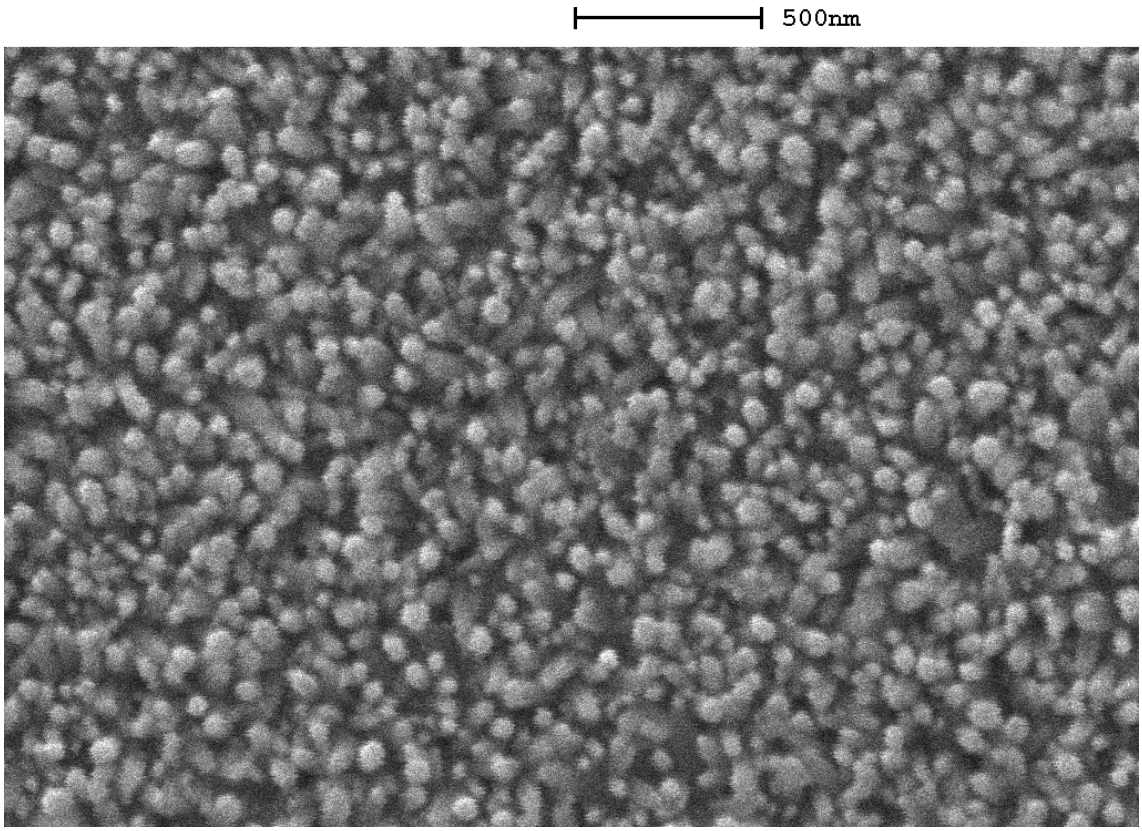

Figure 38 - SEM Image with the seed annealed at 650°C, 40k magnification.

Appendix 4 - EDX O_2 Plasma data

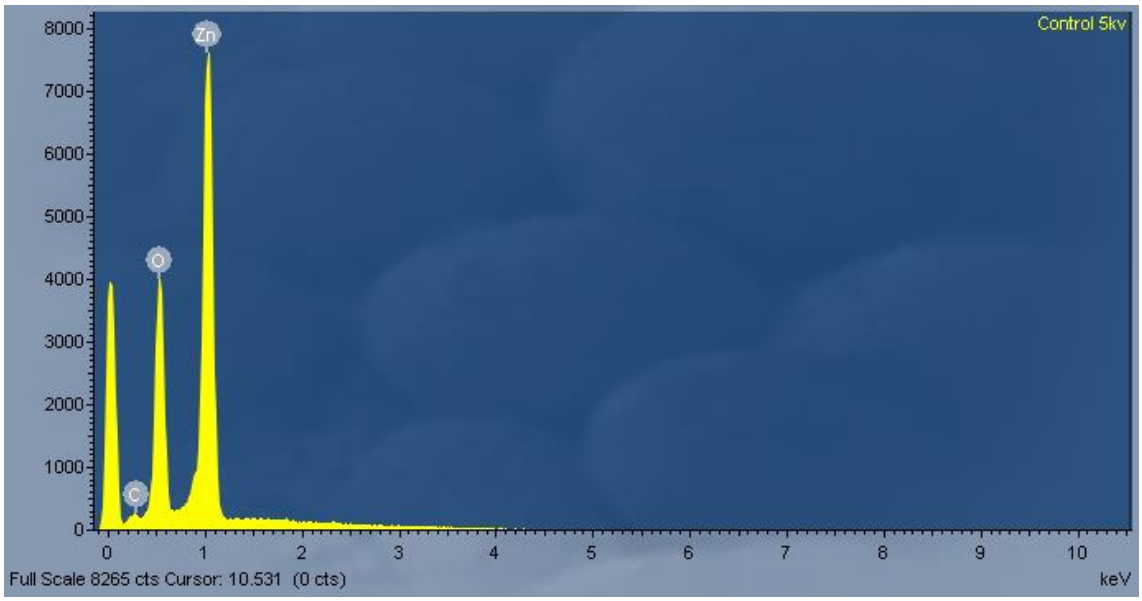

Figure 39 - EDX of the control sample, 5kV.

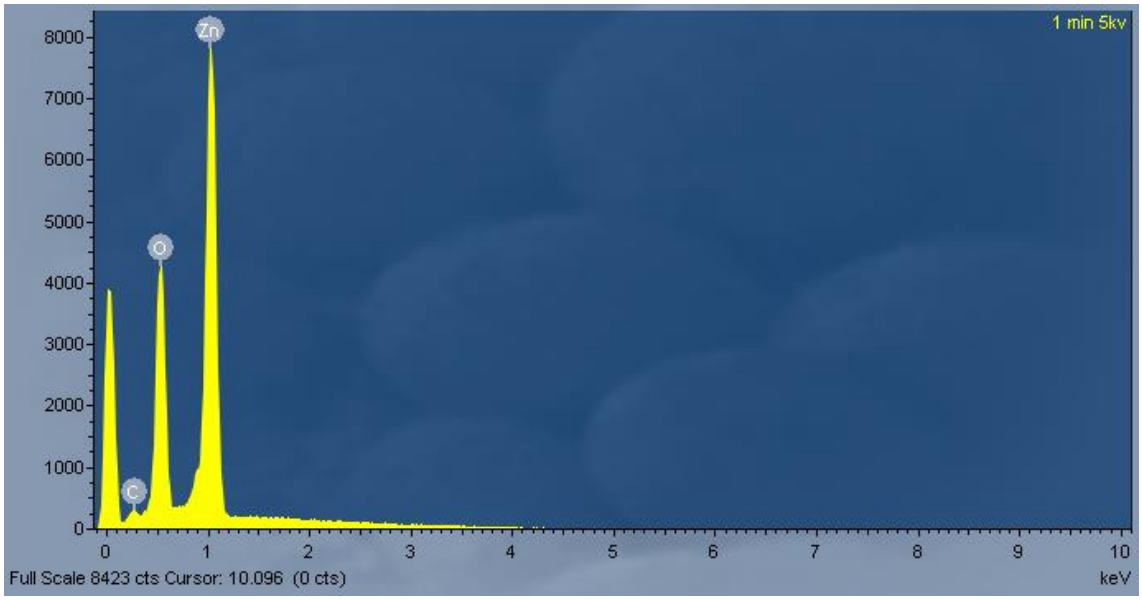

Figure 40 - EDX of the 1 minute sample, 5kV.

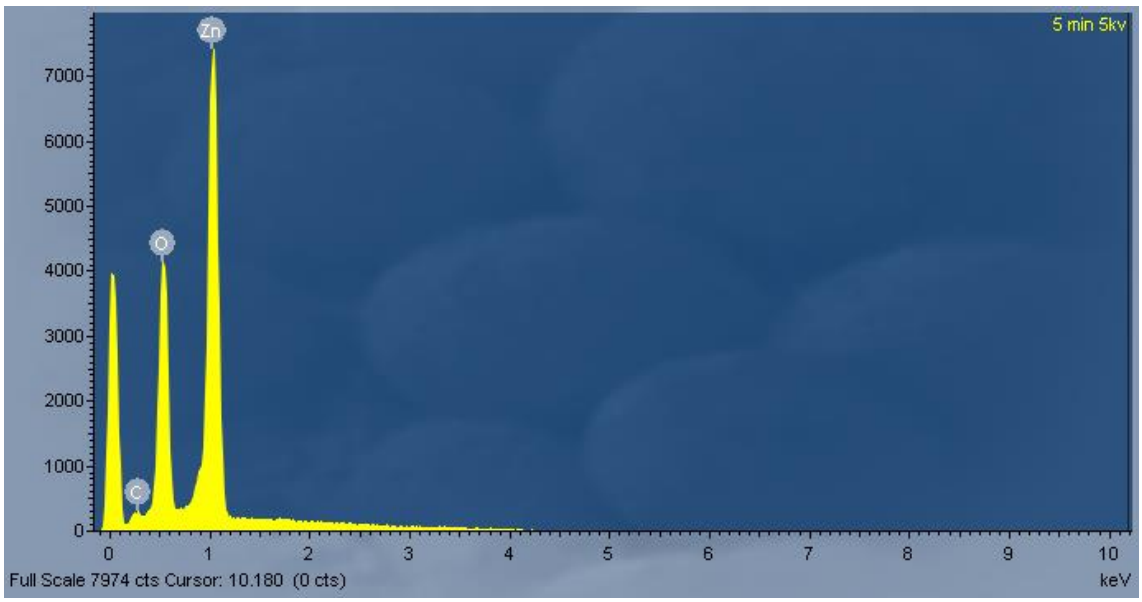

Figure 41 - EDX of the 5 minute sample, 5kV.

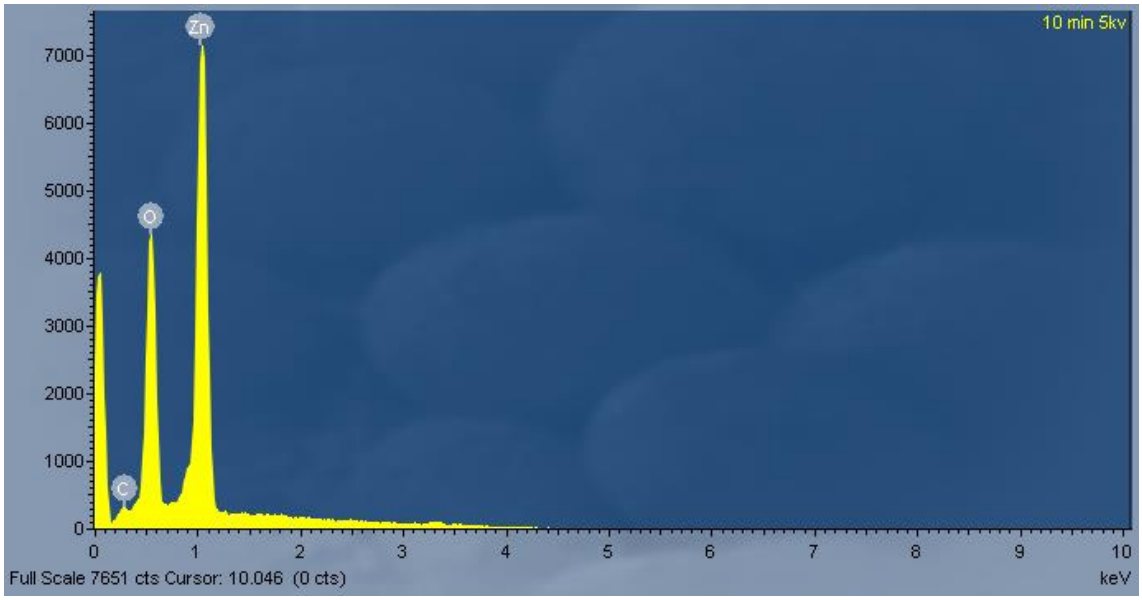

Figure 42 - EDX of the 10 minute sample, 5kV.

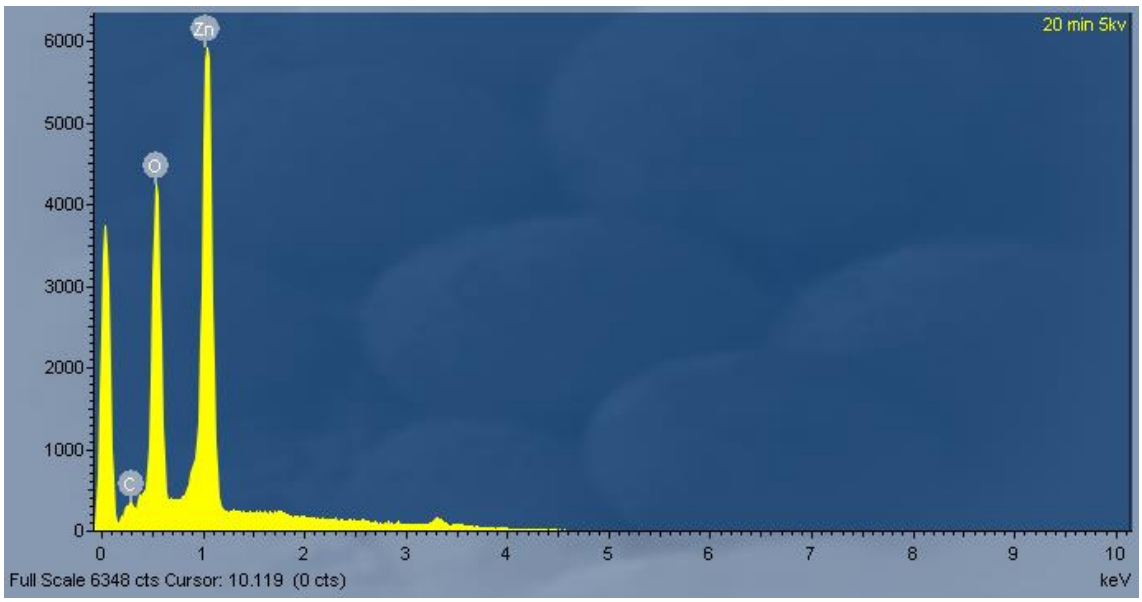

Figure 43 - EDX of the 20 minute sample, 5kV.

Table 4 - All EDX Data.

EDX Data	**Plasma Exposure time (Minutes)**				
Peaks	**0 (Control)**	**1**	**5**	**10**	**20**
Background	3950	3889	3950	3875	3740
Carbon	266	300	300	325	340
Oxygen	4000	4275	4150	4340	4240
Zinc	7600	7805	7425	7150	5920
Silicon (from the substrate)	No Visible Peak				

Appendix 5 - SEM of O_2 Plasma slides

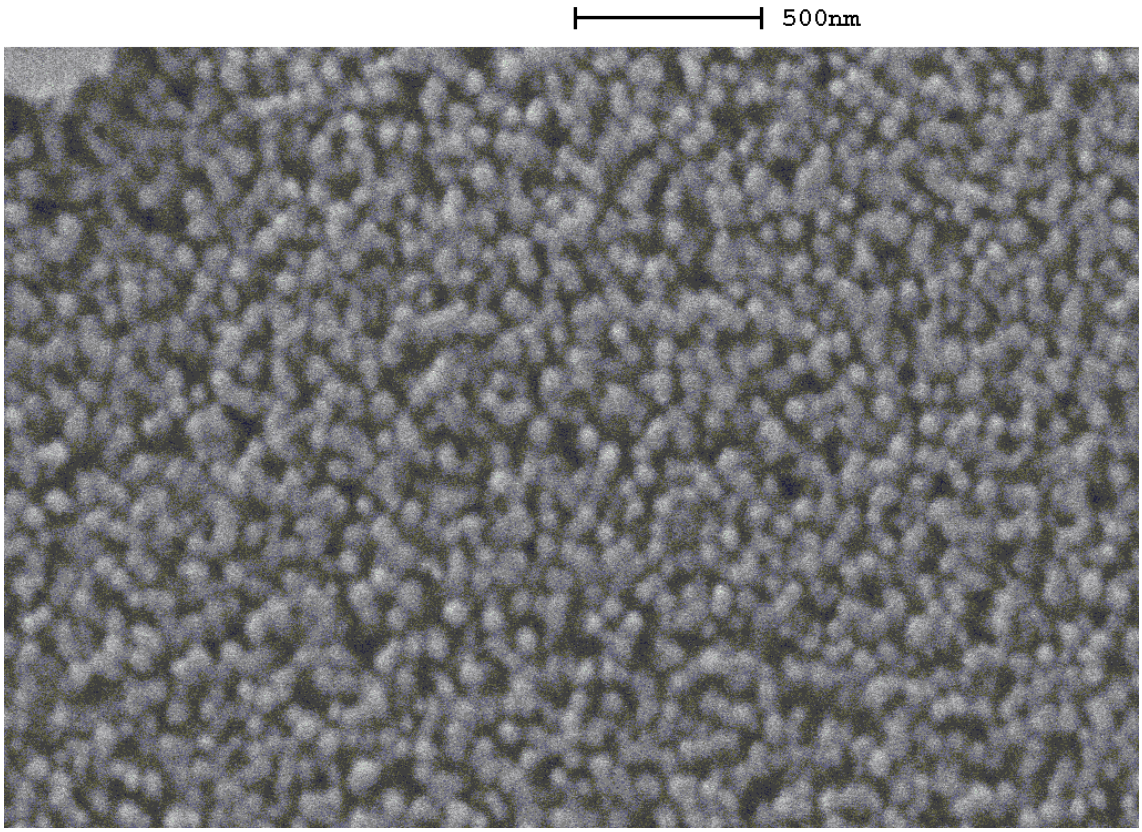

Figure 44 - SEM of the control sample for O_2 Plasma, 40k magnification.

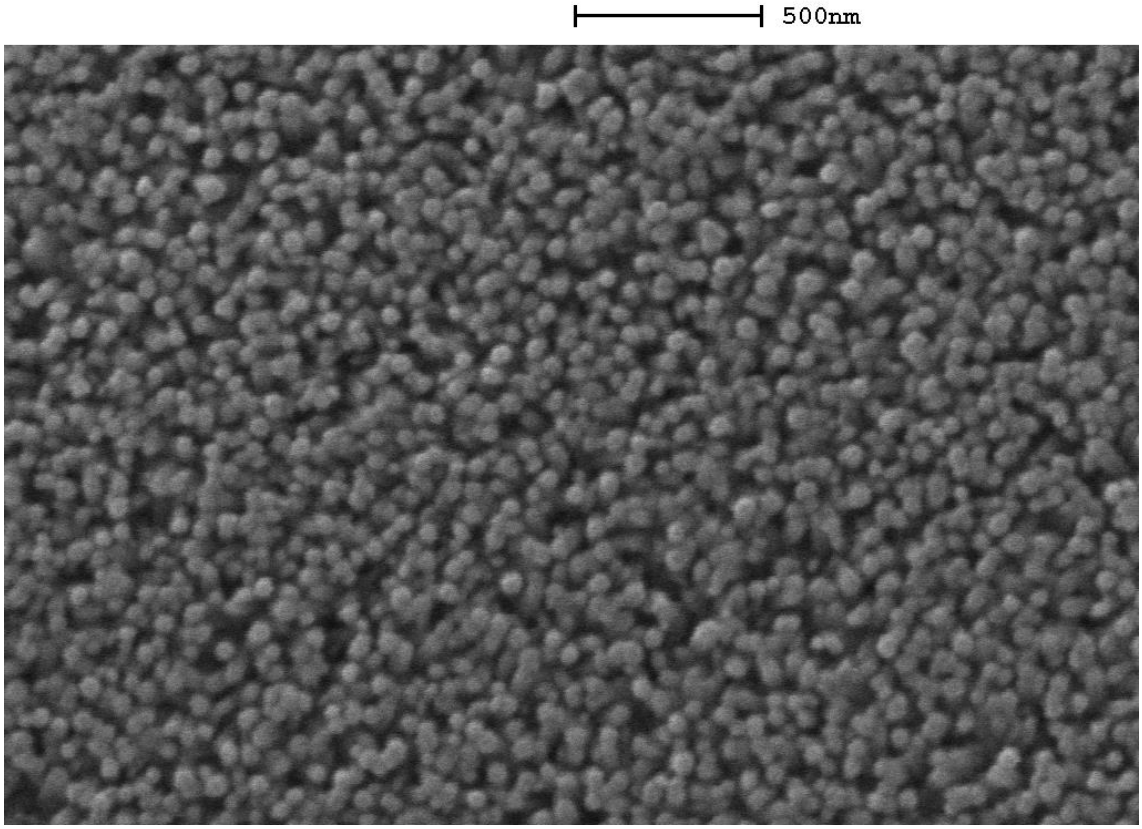

Figure 45 - SEM of the 1 minute sample for O_2 Plasma, 40k magnification.

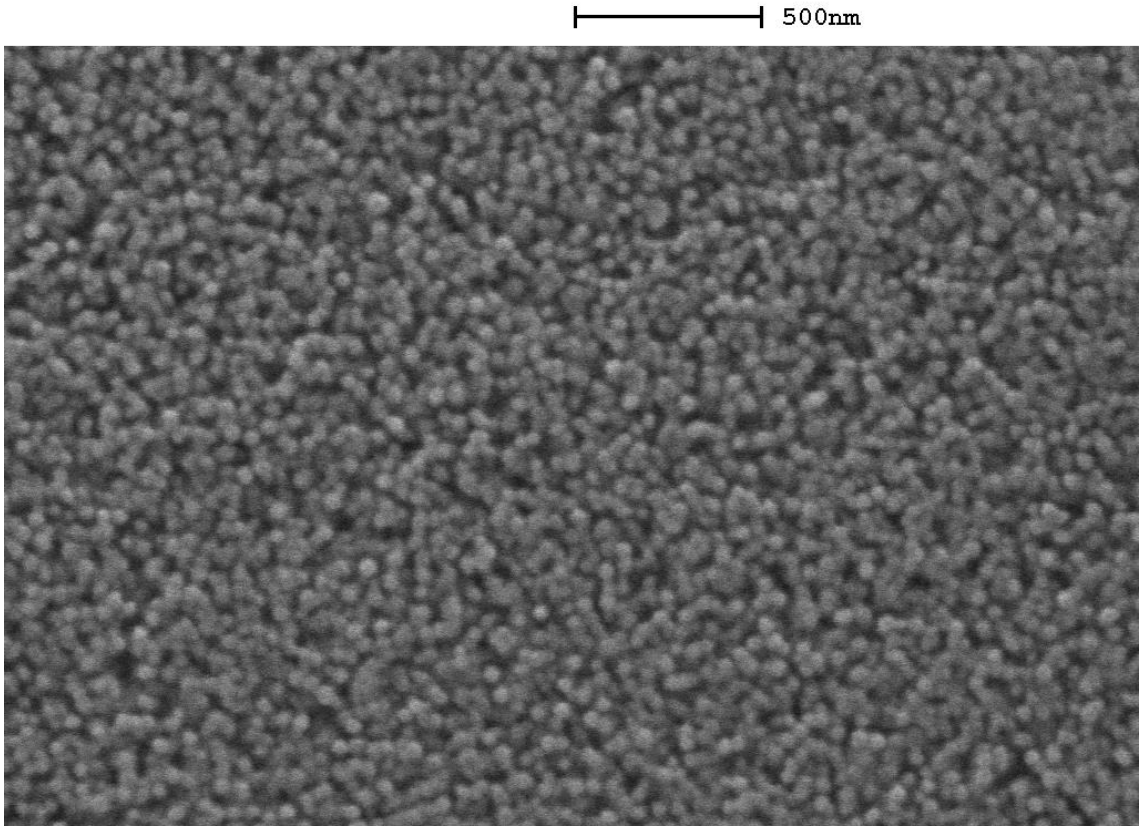

Figure 46 - SEM of the 5 minute sample for O_2 Plasma, 40k magnification.

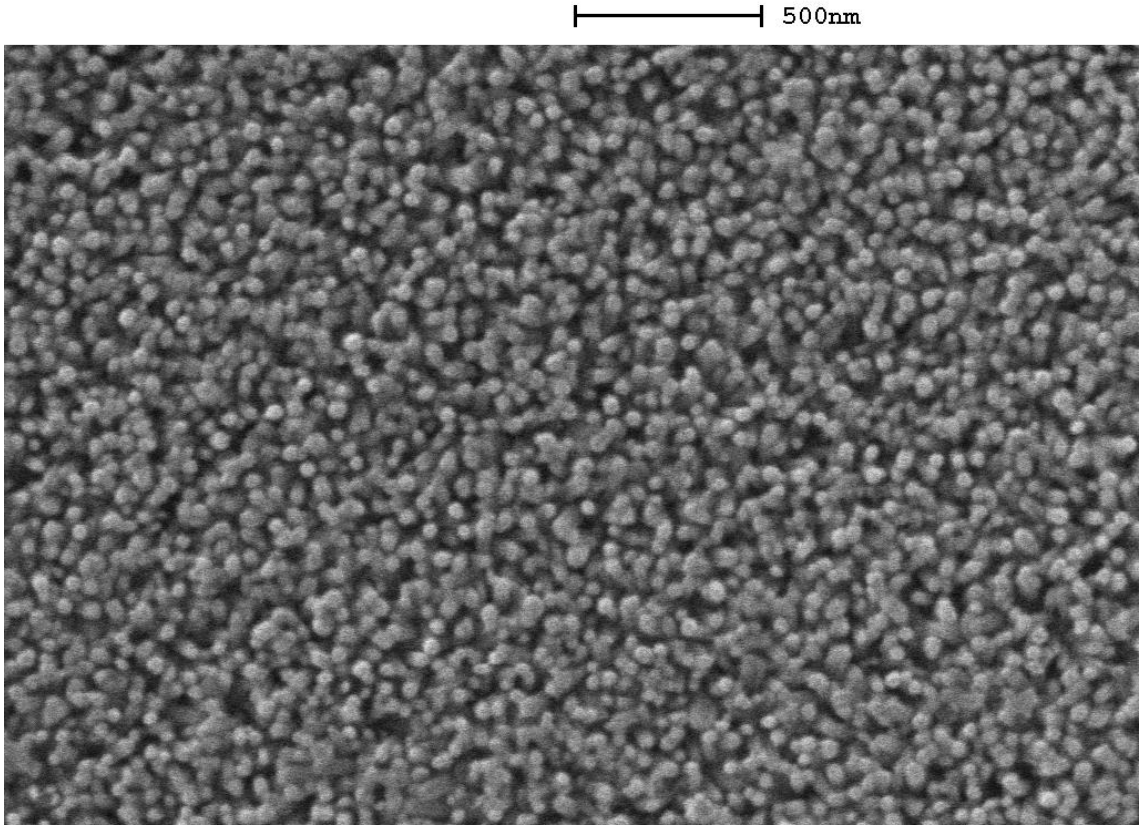

Figure 47 - SEM of the 10 minute sample for O_2 Plasma, 40k magnification.

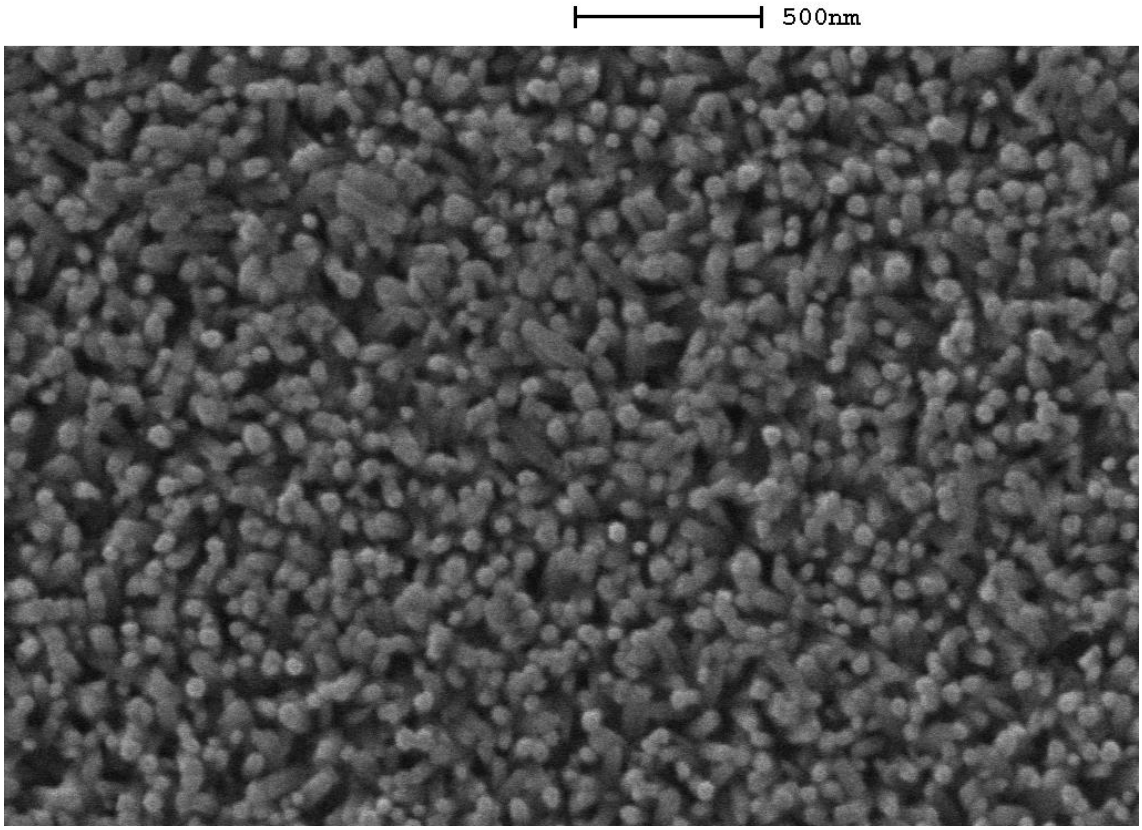

Figure 48 - SEM of the 20 minute sample for O_2 Plasma, 40k magnification.

Appendix 6 - XRD O_2 Plasma Data

Table 5- All XRD O2 Plasma Data.

°2θ	1 min	5 min	10 min	20min	Control	
0,0,2	34.4445	34.4445	34.4445	34.4051	34.4445	
1,0,3	62.8453	62.8059	62.8453	62.8059	62.8453	
0,0,4	72.5748	72.5354	72.5748	72.5748	72.5748	
Planar spacing = d = nλ/2sinθ (Å)			**λ = copper k-alpha-1 line = 1.54056Å**			
0,0,2	2.60159	2.60159	2.60159	2.60448	2.60159	
1,0,3	1.47747	1.47831	1.47747	1.47831	1.47747	
0,0,4	1.30150	1.30211	1.3015	1.3015	1.30150	
	FWHM ° 2θ			**Lattice Parameters**		
	0,0,2	**1,0,3**	**0,0,4**	**a (Å)**	**c (Å)**	**c/a**
Control	0.11279	0.18939	0.11921	3.25498	5.20461	1.59896
1 min	0.11405	0.19972	0.13128	3.25498	5.20461	1.59896
5 min	0.11989	0.48800	0.11999	3.25964	5.20583	1.59705
10 min	0.11156	0.18437	0.12163	3.25498	5.20461	1.59896
20 min	0.19988	0.20862	0.17610	3.25688	5.20750	1.59892

[1] Hayes B, 2011, The Memristor, American Scientist Vol 99 Num 2 Pg 106, DOI: 10.1511/2011.89.106

[2] International Technology Roadmap for Semiconductors (ITRS), White Paper: “Emerging Research Devices”, 2011 Ed

[3] Chua L O, 1971, Circuit Theory, IEEE Transactions on Vol. 18, Issue 5, 507 - 519

[4] Strukov D B, Snider G S, Stewart D R, and Williams R.S, 2008, Nature Vol 453, 80 - 83

[5] U.S. Patient 7,359,888, Snider G S, Hewlett-Packard Development Company

[6] U.S. Patient 8,416,604, Chua L O, Kim H, Industrial Cooperation Foundation Chonbuk National University

[7] Myoung-Jae Lee, Chang Bum Lee, Dongsoo Lee, Seung Ryul Lee, Man Chang, Ji Hyun Hur, Young-Bae Kim, Chang-Jung Kim, David H. Seo, Sunae Seo, U-In Chung, In-Kyeong Yoo & Kinam Kim, 2011, Nature Materials 10, 625–630, doi:10.1038/nmat3070

[8] Martin Flink, June 2014, www8.hp.com/hpnext/posts/discover-day-two-future-now-machine-hp#.VA9MavldV1H

[9] Jon Fingas, July 2014, http://www.engadget.com/2014/06/11/hp-the-machine/

[10] Curtis O’Kelly, Jessamyn A. Fairfield, and John J. Boland, A Single Nanoscale Junction with Programmable Multilevel Memory, Vol’ 8 No’ 11 11724-11729, 2014, ACS Nano.

[11] Sung Hyun Jo, Ting Chang, Idongesit Ebong, Bhavitavya B. Bhadviya, Pinaki Mazumder, and Wei Lu, Nanoscale Memristor Device as Synapse in

Neuromorphic Systems, DOI: 10.1021/nl904092h, Nano Lett. 2010, 10, 1297-1301

[12] Moore, Gordon E. (1965). "Cramming more components onto integrated circuits" Electronics Magazine. http://www.cs.utexas.edu/~fussell/courses/cs352h/papers/moore.pdf

[13] Clark, Don (July 15, 2015). "Intel Rechisels the Tablet on Moore's Law". Wall Street Journal Digits Tech News and Analysis, http://blogs.wsj.com/digits/2015/07/16/intel-rechisels-the-tablet-on-moores-law/

[14] Bradshaw, Tim (July 16, 2015). "Intel chief raises doubts over Moore's law". Financial Times. http://www.ft.com/cms/s/0/36b722bc-2b49-11e5-8613-e7aedbb7bdb7.html

[15] Chua, L. O. 2013, "Memristor, Hodgkin–Huxley, and Edge of Chaos", Nanotechnology 24, 383001, (14pp)

[16] Chua, L. O. 2011, "Resistance switching memories are memristors", Applied Physics A 102 (4): 765–783

[17] Thangamani.V, Memristor-Based Resistive Random Access Memory: Hybrid Architecture for Low Power Compact Memory Design, Vol.4, No.7, 2014, IISTE, Control Theory and Informatics

[18] Lübben, M., Karakolis, P., Ioannou-Sougleridis, V., Normand, P., Dimitrakis, P. and Valov, I. (2015), Graphene-Modified Interface Controls Transition from VCM to ECM Switching Modes in Ta/TaO_x Based Memristive Devices. Adv. Mater., 27: 6202–6207. doi:10.1002/adma.201502574

[19] T.W. Hickmott, J. Appl. Phys., 33 (1962), p. 2669

[20] Stukov D.B. ; Snider G.S. ; Stewart D.R ; Stanley Williams R., The missing memristor found, Nature 453 pp. 80-83 (2008)

[21] Matthew D. Pickett, Dmitri B. Strukov, Switching dynamics in titanium dioxide memristive devices, Journal of Applied Physics 106, 074508 (2009)

[22] Strukov D B, Snider G S, Stewart G R and Williams R S,2008, *Nature* 453, 80

[23] Wang Xiao-Ping, Chen Min, and Shen Yi, Switching mechanism for TiO2 memristor and quantitative analysis of exponential model parameters, Published 20 June 2015, 2015 Chinese Physical Society and IOP Publishing Ltd, Chinese Physics B, Volume 24, Number 8

[24] Yang J J, Pickett M D, Li X, Ohlberg D A, Stewart D R and Williams R S, 2008, Nat. Nanotechnol. 3, 429

[25] M. Janousch, G. I. Meijer, U. Staub, B. Delley, S. F. Karg, and B. P. Andreasson, Adv. Mater, Weinheim, Ger. 19, 2232, 2007. 1

[26] C. Klingshirn, R. Hauschild, H. Priller, M. Decker, J. Zeller, H. Kalt, ZnO rediscovered once again!?, Superlattices and Microstructures 38 (2005) 209–222

[27] Akira Onodera and Masaki Takesada (2012). Electronic Ferroelectricity in II-VI Semiconductor ZnO, Advances in Ferroelectrics, Dr. Aimé Peláiz-Barranco (Ed.), ISBN: 978-953-51-0885-6, InTech, DOI: 10.5772/52304. Available from: http://www.intechopen.com/books/advances-in-ferroelectrics/electronic-ferroelectricity-in-ii-vi-semiconductor-zno

[28] Fu-Chien Chiu, 2014, Materials 2014, 7, 7339-7348

[29] Bin Zhang, Yu Chen, Koon-Gee Neoh, and En-Tang Kang, Organic Electronic Memory Devices, doi:10.1039/9781782622505-0000

[30] Ma, D., Aguiar, M., Freire, J. A. & Hümmelgen, I. A. 2000 Organic reversible switching devices for memory applications. Adv. Mater. 12, 1063–1066.

[31] Liping Ma, Jie Liu, Seungmoon Pyo, Qianfei Xu & Yang Yang (2002) Organic Bistable Devices, Molecular Crystals and Liquid Crystals, 378:1, 185-192, DOI:10.1080/713738589

[32] Greene L E, Law M, Goldberger J, Kim F, Johnson J C, Zhang Y, Saykally R J and Yang P D 2003 Angew. Chem. Int. Edn 42 3031

[33] Greene L E, Yuhas B D, Law M, Zitoun D and Yang P 2006 Inorg. Chem. 45 7535

[34] Greene L E, Law M, Tan D H, Montano M, Goldberger J, Somorjai G, Yang P 2005 Nano Letters Vol. 5 No. 7, 1231 – 1236

[35] Unalan HE, Hiralal P, Rupesinghe N, Dalal S, Milne W I and Amaratunga G A J , 2008 Nanotechnology 19 255608

[36] Schepütz C M, Yang Y, Husseini N S, Heinhold R, Kim H-S, Allen M W, Durbin S M, and Clark R. 2012, IOP Publishing, J. Phys.: Condens. Matter 24, 095007

[37] Faber H, Hirschmann J, Klaumünzer M, Braunschweig B, Peukert W, and Halik M, ACS Appl. Mater. Interfaces, 2012, 4 (3), pp 1693–1696

[38] Chi-Ken Lu and Hsin-Fei Meng, 2007, Hole doping by molecular oxygen in organic semiconductors: Band-structure calculations, Phys. Rev. B 75, 235206

[39] Greene L E, Law M, Tan D H, Montano M, Goldberger J, Somorjai G, Yang P, 2005 Nano Letters Vol. 5 No. 7, 1231 – 1236

[40] Lin C, Li Y, 2008, Synthesis of ZnO nanowires by thermal decomposition of zinc acetate dehydrate, Materials Chemistry and Physics, Volume 113, Issue 1, 15 January 2009, Pages 334–337

[41] Kevin M. McPeak, Thinh P. Le, Nathan G. Britton, Zhorro S. Nickolov, Yossef A. Elabd, and Jason B. Baxter, Langmuir 2011, 27, 3672–3677

[42] Russell Hobbs Instruction manual for the RHM2507 microwave, http://mda.russellhobbs.com/IBS/RHM2507.pdf

[43] Boruoushian M, Kosanovic T, Scientific Research Crystal Structure Theory and Applications, 2012, 1, 35-39

[44] Prime D, and Paul S, Phil. Trans. R. Soc. A 28 October 2009 vol. 367 no. 1905 4141-4157

[45] Greene L E, Law M, Tan D H, Montano M, Goldberger J, Somorjai G, Yang P, 2005 Nano Letters Vol. 5 No. 7, 1231 – 1236

[46] Bhat D K, 2007, Nanoscale Research Letters, Facile Synthesis of ZnO Nanorods by Microwave Irradiation of Zinc–Hydrazine Hydrate Complex

[47] Akhtar MJ, Ahamed M, Kumar S, Khan MM, Ahmad J, Alrokayan SA, 2012, Zinc oxide nanoparticles selectively induce apoptosis in human cancer cells through reactive oxygen species, International Journal of Nanomedicine,.

[48] Zhang Y, Ram M K, Elias S K, and Goswami Y, 2012, Journal of Nanomaterials, ID 624520

[49] Kaye and Laby, Wurtzite crystal structure, c/a value 1.633, National Physical Laboratory, 2014, http://www.kayelaby.npl.co.uk/chemistry/3_7/3_7_7.html

[50] International Tables for Crystallography, Mathematical, Physical and Chemical Tables, E. Prince, International Union of Crystallography, Springer Science & Business Media, 22 Mar 2004, Table 5.2.11.1. NIST intensity standards, SRM 674, page 503

[51] Zheng Zhong-Kui, Duanmu Qing-Duo, Zhao Dong-Xu, Wang Li-Dan, Shen De-Zhen, 2012, The Annealing-Induced Shape Deformation of Hydrothermal-Grown ZnO Nanorods, Chinese Physics Letters, vol. 29, No.1, 017804

[52] UQG Optics Data Sheet for ITO Glass Windows, Product number GTO-2521, Dimensions 25mm x 25mm, www.uqgoptics.com/pdf/ITO%20Glass.pdf

[53] Toru Mitsunaga, 2009, X-ray thin-film measurement techniques II, Rigaku Journal, RJ25-1_7-12, Volume 25.

[54] J. F. Huang; C. K. Xia; L. Y. Cao; X. R. Zeng; J. P. Wu; H. Y. He, Growth conditions for zincite zinc oxide nanocrystallites in aqueous solutions by microwave hydrothermal process, Materials Research Innovations, Volume 12, Issue 4 (01 December 2008), pp. 200-209

[55] Simple Preparation and Characterization of Nano-Crystalline Zinc Oxide Thin Films by Sol-Gel Method on Glass Substrate, Muhammad Saleem, Liang Fang, Aneela Wakeel, M. Rashad, C. Y. Kong, World Journal of Condensed Matter Physics, 2012, 2, 10-15

[56] Christopher J. Ward, Robert Tronndorf, Alicia S. Eustes, Maria L. Auad, and Edward W. Davis, Seed-Mediated Growth of Gold Nanorods: Limits of Length to Diameter Ratio Control, Journal of Nanomaterials, Volume 2014 (2014), Article ID 765618, 7 pages

[57] Liu J-b, Chen S, Wu Z-q, Xiao Z-b, Zhang Y-k, and Huang B-y, 2003, Journal of Central South University of Technology, Issue 1, Vol. 10, 49 – 52